Novel If1 mechanism preventing ATP hydrolysis by the ATP synthase subcomplex in *Saccharomyces cerevisiae*.

Orane Lerouley[1], Isabelle Larrieu[1], Tom Louis Ducrocq[1], Benoît Pinson[1,2], Marie-France Giraud[3] and Arnaud Mourier[1]*

[1] University of Bordeaux, CNRS, IBGC, UMR 5095, 33000 Bordeaux, France.
[2] Metabolic Analyses Service, TBMCore-Université de Bordeaux-CNRS UAR 3427-INSERM US005, Bordeaux, France.
[3] Univ. Bordeaux, CNRS, Bordeaux INP, CBMN, UMR 5248, F-33600 Pessac, France

Orane Lerouley *0009-0000-2514-0964*
Benoît Pinson *0000-0003-2936-9058*
Tom Louis Ducrocq *0009-0009-6148-4057*
Marie-France Giraud. *0000-0002-6238-667X*
Arnaud Mourier *0000-0002-5413-611X*

* For correspondence

Arnaud Mourier
1, rue Camille Saint-Saëns
33077 Bordeaux
arnaud.mourier@ibgc.cnrs.fr

Abstract

The mitochondrial F_1F_0-ATP synthase is crucial for maintaining the ATP/ADP balance which is critical for cell metabolism, ion homeostasis, cell division, proliferation and motility. This enzyme, conserved across evolution, is found in the mitochondria or chloroplasts of eukaryotic cells and the plasma membrane of bacteria. *In vitro* studies have shown that the mitochondrial F_1F_0-ATP synthase is reversible, capable of hydrolyzing instead of synthesizing ATP. *In vivo*, its reversibility is inhibited by the endogenous peptide If1 (Inhibitory Factor 1), which specifically prevents ATP hydrolysis in a pH-dependent manner. Despite its presumed importance, the loss of If1 in various model organisms does not cause severe phenotypes, suggesting its role may be confined to specific stress or metabolic conditions yet to be discovered. In this study, we explored the structural and physiological importances of If1 inhibitory peptides in *Saccharomyces cerevisiae*. Our analyses indicate that inhibitory peptides are crucial in mitigating metabolic adverse outcomes caused by mitochondrial depolarizing stress under glyco-oxidative metabolic conditions. Under glyco-oxidative metabolic state, the energy maintenance relies both on glycolysis and oxidative phosphorylation. Additionally, we found that the absence of If1 destabilizes the nuclear-encoded free F_1 subcomplex. This novel mechanism of action highlights the role of If1 in preventing harmful ATP wastage, offering new insights into its function under physiological and pathological conditions.

Introduction

The mitochondrial F_1F_0-ATP synthase is among the most advanced molecular enzymatic nanomachines in the living word. This enzyme is highly evolutionary conserved (Sinha and Wideman, 2023), and ubiquitous in the mitochondria or chloroplasts of eukaryotic cells, as well as in the plasma membrane of bacteria (Lau et al., 2008; Hahn et al., 2018; Gu et al., 2019; Pinke et al., 2020; Yang et al., 2020; Courbon and Rubinstein, 2022). This multisubunit enzyme is a cornerstone of the oxidative phosphorylation system (OXPHOS) as it transduces the proton electrochemical gradient ($\Delta\mu H^+$) generated by the respiratory chain, to synthesize ATP from ADP and inorganic phosphate (Mitchell, 1961; Boyer et al., 1973; Stock et al., 1999; Watt et al., 2010). In *Saccharomyces cerevisiae*, this 600 kDa enzyme comprises a catalytic domain F_1 ($\alpha_3\beta_3\gamma_1\delta_1\varepsilon_1$) and a F_0 region, divided into a membranous rotor (subunit (su) 9_{10}-ring) and a peripheral stalk (su 4, su 6, su 8, su f, OSCP, su d, su h, su i/j) that connects the catalytic head to the rotor ring. Three additional subunits, su e, su g and su k are involved in enzyme dimerization. Proton translocation across two hemi-channels at the interface of su 6 and the membranous ring induces ring rotation, that triggers the rotation of a central stalk (γ,δ,ε) inside the two catalytic subunits (α and β), enabling conformational changes required for ATP synthesis. The eukaryotic F_1F_0-ATP synthases are composed of 17 different subunits, encoded by the nuclear (nDNA) or mitochondrial genome (mtDNA) (Senior, 1988; Kühlbrandt, 2019). The dual genetic origin of the F_1F_0-ATP synthase implies that gene expression from both genomes must be tightly coordinated to ensure proper biogenesis and assembly of the enzyme. Nevertheless, in cells presenting defective mitochondrial genome levels and expression or impaired ATP synthase assembly, F_1 is commonly found assembled as a stable subcomplex capable of ATP hydrolysis (Tzagoloff, 1969; Carrozzo et al., 2006; Wittig et al., 2010). The F_1F_0-ATP synthase, along with glycolysis and other pathways that allow substrate-level phosphorylation, is critical in maintaining the ATP/ADP balance, which is required for cell metabolism, ion homeostasis, cell division, proliferation and motility. In multicellular organisms, mitochondrial ATP synthesis is finely adjusted to sustain specialized functions of differentiated cells, and in humans, defective OXPHOS-driven ATP synthesis causes multiple and severe diseases frequently affecting high-energy demanding tissues such as cardiac and skeletal muscles, as well as the nervous system (Galber et al., 2021).

Interestingly, the mitochondrial F_1F_0-ATP synthase is fully reversible and *in vitro* experiments performed on purified enzymes or functional mitochondria demonstrated that ATP hydrolysis could be coupled to proton translocation, generating a proton

electrochemical potential across the inner mitochondrial membrane (Boyer et al., 1973; Pietrobon et al., 1983; Mourier et al., 2010). However, the reversibility of the F_1F_0-ATP synthase is, under physiological conditions, prevented by the membrane potential generated by the respiratory chain and is only observed when the respiratory chain is blocked (chemical inhibitor or anoxia), or when the proton electrochemical membrane potential is abolished. The reversibility of the F_1F_0-ATP synthase is also regulated by a nuclear encoded inhibitory peptide, so called inhibitory factor 1 (If1), which can physically interact and inhibit the F_1 catalytic domain (Pullman and Monroy, 1963). Since its discovery, homologs of If1 were found and characterized in other species (Cintrón and Pedersen, 1979; Hashimoto et al., 1981; Matsubara et al., 1981; Norling et al., 1990; Ichikawa and Ogura, 2003). The If1 amino acid sequences are well conserved across evolution, and for yet unclear reasons, two homologous inhibitory peptides, namely If1 and Stf1 (Stabilizing Factor 1), presenting redundant activity were identified in *S. cerevisiae* (Hashimoto et al., 1987; Cabezon et al., 2002; Venard et al., 2003). If1 and Stf1 proteins are encoded respectively by *INH1* and *STF1* nuclear gene in *S. cerevisiae*. An important wealth of experiments on independent eukaryote models have contributed to characterize the mechanism of action (Pullman and Monroy, 1963; Hashimoto et al., 1981, 1984; Cabezon et al., 2000, 2002; Venard et al., 2003), as well as the structural interaction of these peptide inhibitors with the F_1F_0-ATP synthase (Cabezón et al., 2001; Robinson et al., 2013; Boreikaite et al., 2019; Gu et al., 2019; Mühleip et al., 2021; Romero-Carramiñana et al., 2023). One of the most remarkable and evolutionary conserved features of If1 inhibition is its regulation by pH, being optimal under neutral or slightly acidic pH conditions and inactive at pH above 8.0 (Pullman and Monroy, 1963; Hashimoto et al., 1987). The pH-dependent If1 inhibition of F_1F_0-ATP synthase strikingly aligns and supports its function, potentiating its capacity to prevent ATP hydrolysis under depolarization when the ΔpH is abolished. Interestingly, the importance of If1 under genetic or chemical stress preventing maintenance of the membrane potential by the respiratory chain has been confirmed in various model organisms (Buchet and Godinot, 1998; Rouslin and Broge, 1996; Sgarbi et al., 2018; Venard et al., 2003).

The Cryo-EM structures of oligomeric F_1F_0-ATP synthases demonstrated that If1 dimers, could bridge adjacent F_1F_0-ATP synthase dimers, suggesting that If1 could stabilize oligomers (Cabezón et al., 2000; Pinke et al., 2020; Gu et al., 2019). Functional investigations in mammalian cells and mouse models supported the idea that If1 regulates F_1F_0-ATP synthase oligomerization (Domínguez-Zorita et al., 2023) and even suggested that If1 could also regulate ATP synthesis (García-Bermúdez et al., 2015; Sánchez-Cenizo et al., 2010). However, the role of If1 in controlling F_1F_0-ATP synthase oligomerization and

ATP synthesis activity remains debated and needs to be confirmed in other model organisms (Dienhart et al., 2002; Lucero et al., 2021; Gatto et al., 2022; Carroll et al., 2024; Galkina et al., 2022). The current controversy over the role of If1 in energy metabolism partly arises from the lack of methods to monitor, *in vivo*, ATP hydrolysis by the mitochondrial ATP synthase operating in reverse. Furthermore, the absence of major phenotypes associated with If1 loss in many organisms suggests that its action may be limited to specific stress or metabolic conditions that remain to be discovered (Ichikawa et al., 1990; Nakamura et al., 2013; Fernández-Cárdenas et al., 2017).

The goal of our study was to clarify the structural and physiological roles of inhibitory peptide If1/STF1 in the yeast *S. cerevisiae*. Our analyses demonstrate that the If1/Stf1 activity is dispensable to sustain the growth of yeast under 'respiro-fermentative' or 'respiratory strict' carbon sources. However, we observed that inhibitory peptides are key in sustaining growth of yeast subjected to mitochondrial depolarizing stress under glyco-oxidative metabolic conditions. We also hereby demonstrate that loss of inhibitory peptides does not impact high supramolecular organization of the yeast F_1F_0-ATP synthase but surprisingly destabilizes the free F_1 subcomplex. This discovery prompted us to revisit the role of the free F_1 subcomplex to sustain the ability for *S. cerevisiae* to grow in total or partial absence of mitochondrial genome ($\rho^{-/\circ}$).

Results

If1/Stf1 inhibitors are required to maintain the ATP synthase free F_1 subcomplex.

Independent works have previously established that *S. cerevisiae* expresses two F_1F_0-ATP synthase inhibitory peptides named If1 and Stf1, respectively encoded by the genes *INH1* and *STF1* (Ichikawa et al., 1990; Hashimoto et al., 1990). Therefore, to investigate the role of F_1F_0-ATP synthase endogenous inhibitory peptides on yeast energy producing system and metabolism, we generated an *inh1*Δ *stf1*Δ double knockout strain. The complete loss of If1 and Stf1 was validated by Western blot analyses performed on total protein extracts from yeast harvested during exponential growth on non-fermentable carbon source (glycerol 2%) (Figure 1A). We observed that the individual or combined loss of the peptide inhibitors did not affect the growth on respiratory strict carbon sources such as lactate (2%) (Figure 1B). This unaltered growth on lactate carbon source, which depends on mitochondrial OXPHOS content and activity (Devin et al., 2006), suggested that the loss of If1 and Stf1 did not strongly affect OXPHOS capacities under physiological conditions. We then performed classical native polyacrylamide gel electrophoresis (PAGE) to characterize the supramolecular assembly of the F_1F_0-ATP synthase in *inh1*Δ *stf1*Δ purified mitochondria (Figure 1C). The in-gel ATPase activity demonstrated that, in line with

previous reports (Dienhart et al., 2002), the F_1F_0-ATP synthase monomers (V) and dimers were unchanged in *inh1*Δ *stf1*Δ. Interestingly, our native PAGE experiments demonstrate that levels of higher F_1F_0-ATP synthase oligomers were not impacted by the combined loss of both If1 and Stf1 (Figure 1C). However, in contrast to the F_1F_0-ATP synthase oligomers, we noticed that the free F_1 subcomplex level was almost undetectable in *inh1*Δ *stf1*Δ. The free F_1 subcomplex used to be frequently interpreted as a degradation or destabilization byproduct of the F_1F_0-ATP synthase monomers or dimers, potentially occurring during mitochondrial isolation or detergent solubilization. To minimize the risk of degradation, we decided to characterize the F_1F_0-ATP synthase supramolecular organization on total soluble protein extract bypassing potential mitochondrial degradation inherent to the fastidious mitochondrial isolation procedure. Despite dampening the resolution and characterization of high molecular weight complexes, blue native PAGE (BN-PAGE) performed on total cell extracts confirmed that free F_1 subcomplex was present in control yeast but lost in *inh1*Δ *stf1*Δ (Figure 1D). Intriguingly, in contrast to the F_1F_0-ATP synthase monomers and oligomers levels, the free F_1 subcomplex was clearly detected in WT under BN-PAGE and hardly visible under clear native PAGE (CN-PAGE) conditions. This observation prompted us to determine if the free F_1 subcomplex observed in BN-PAGE could result from (i) the potential impact of the Coomassie brilliant blue on destabilization of the fully assembled complexes (V and oligomers) or (ii) the fact that migration of the free F_1 relies on its binding to the charged Coomassie dye. To this end we performed CN or BN-PAGE to characterize the F_1F_0-ATP synthase assemblies present in digitonin solubilized proteins in (i) total cell extracts, (ii) total cell membrane extracts and (iii) total cell soluble fraction (Figure 1E). As expected, the membrane and soluble fractionation could efficiently separate the membrane-anchored fully assembled ATP synthase from the membrane-free F_1 subcomplex, confirming that the free F_1 subcomplex is a soluble entity. Moreover, the absence of the free F_1 subcomplex in the solubilized membrane extracts demonstrated that this subcomplex is not a destabilization byproduct of the fully assembled ATP synthase post solubilization. Our conclusion, supporting that free F_1 subcomplex is not a destabilization byproduct was strengthened by the titration of the ratio between digitonin and mitochondrial protein (Figure S1A and B). We observed that the progressive increase in digitonin to protein ratio gradually destabilized oligomers, but did not impact the levels of free F_1 subcomplex detected in WT or in *inh1*Δ *stf1*Δ. Consequently, the faint level of free F_1 observed in all extracts subjected to CN-PAGE suggested that the migration of the soluble free F_1 subcomplex is heavily conditioned by the Coomassie-conferred charge (Figure 1E). In line with the result obtained previously (Figure 1D-F), BN-PAGE analysis of total protein showed that the F_1 subcomplex level

was more severely reduced in *inh1*Δ than in *stf1*Δ, and was hardly detected in *inh1*Δ *stf1*Δ (Figure 1D-F). Altogether, our analyses clearly indicate that the amounts of free soluble F_1 subcomplex rely on If1 and to a lower extend on Stf1.

If1 binds and inhibits ATP synthase oligomers, monomers and free F_1 subcomplex.

The intriguing interdependency between If1/Stf1 and free F_1 subcomplex prompted us to further investigate the interplay between these factors. First, to gain structural insights into the interaction between If1 and the mitochondrial F_1F_0-ATP synthase, we performed two-dimensional electrophoresis *i.e* BN-PAGE followed by a second dimensional gel, denaturing SDS-PAGE (Figure 2A). The Western blot experiments confirmed that the entities identified so far through their in-gel ATPase activities (Figure 1C-F), were indeed the mitochondrial F_1F_0-ATP synthase complexes and subcomplexes (Figure 2A) and confirmed the drastic loss of free F_1 in *inh1*Δ *stf1*Δ. Beyond some specific F_1F_0-ATP synthase subunits, we also managed to localize If1 proteins and confirmed that If1 physically interacts with the different F_1F_0-ATP synthase assemblies (Figure 2A and B). Interestingly, the densitometric signal quantification demonstrated that If1 exhibits an even binding capacity toward the different F_1F_0-ATP synthase assemblies (Figure 2B). However, we could not detect or visualize Stf1 in the second dimension. The previously reported lower binding efficiency and affinity of Stf1 for F_1F_0-ATP synthase compared to If1 (Venard et al., 2003), could likely explain the undetectable level of Stf1 following the digitonin extraction and BN-PAGE procedures. Next, we functionally characterized the interplay between If1/Stf1 and F_1F_0-ATP synthase assemblies on non-solubilized samples (Figure 2C-E). The ATP hydrolysis flux measurement performed on total yeast protein extracts confirmed that the pH-dependent inhibition of the ATPase activity was completely abolished in *inh1*Δ *stf1*Δ (Figure 2C). Furthermore, our analyses demonstrated that the oligomycin-sensitive ATPase activity, associated with fully assembled F_1F_0-ATP synthase, assessed in WT and *inh1*Δ *stf1*Δ samples were identical (Figure 2D). In contrast, the oligomycin-insensitive ATPase activity, mainly related to free F_1 subcomplex, was drastically reduced in the *inh1*Δ *stf1*Δ strain (Figure 2D). The complete oligomycin insensitivity of the ATP hydrolysis activity assessed in the soluble fraction (Figure 2E), containing exclusively free F_1 subcomplexes (Figure 1E), confirmed that the oligomycin-resistance was inherent to free F_1 subcomplexes. Interestingly, the oligomycin-resistant ATPase activity of free F_1 subcomplexes was fully inhibited by If1/Stf1 through their characteristic pH-dependent inhibition (Figure 2E), confirming their capacity to physically and functionally interact (Figure 2Aand B). This functional characterization nicely corroborates the structural observation showing that WT and *inh1*Δ *stf1*Δ present similar

levels of F_1F_0-ATP synthase monomers and oligomers (Figure 1C and D). Altogether, native PAGE (Figure 1C-F and Figure 2 A-B) and functional analyses (Figure 2D and E) demonstrate that the oligomycin-insensitive free F_1 subcomplex is severely reduce in *inh1*Δ *stf1*Δ.

If1/Stf1 are specifically involved in free F_1 subcomplex stabilization

To further investigate the interplay between the inhibitory peptides If1/Stf1 and the free F_1 subcomplex, we decided to evaluate the stability of the different F_1F_0-ATP synthase assemblies in the *inh1*Δ *stf1*Δ strain. To this end, we characterized the fate of the different ATP synthase assemblies in WT and *inh1*Δ *stf1*Δ strains grown in complete medium containing glycerol (2%) and subjected to a cycloheximide treatment inhibiting cytosolic translation (Buchanan et al., 2016). This experiment clearly showed that a 90-minute treatment did not affect the steady state levels of the inhibitory peptides If1/Stf1 but severely affected, with distinct kinetics, the levels of F_1F_0-ATP synthase assemblies (Figure 3A and B). Interestingly, the destabilization profile of F_1F_0-ATP synthase monomers and oligomers in *inh1*Δ *stf1*Δ was comparable to WT, and the loss of these different entities was not followed by any detectable increase in the free F_1 subcomplex level. To further investigate the importance of If1/Stf1 and free F_1 subcomplex interplay, we decided to investigate how loss of If1 impacts the phenotype of the *atp18*Δ strain lacking the F_1F_0-ATP synthase subunit i/j. This strain was previously characterized and presents a perturbed assembly and fragilized supramolecular organization of the F_1F_0-ATP synthase associated with a profound deficiency in enzyme activity. Loss of subunit i/j was also associated with an increased free F_1 subcomplex and oligomycin-insensitive activity (Vaillier et al., 1999; Wagner et al., 2010). The CN and BN-PAGE performed on the solubilized ATP synthase from total protein cell extracts of the *atp18*Δ mutant confirmed previous observations demonstrating that the levels of F_1F_0-ATP synthase oligomers were severely destabilized whereas the levels of free F_1 subcomplex were strongly increased (Figure 3C). Interestingly, in contrast to the loss of stf1, loss of If1 in the *atp18*Δ strain affected drastically the level of the free F_1 subcomplex without affecting the levels of the monomeric F_1F_0-ATP synthase (Figure 3C, D and E). The predominant role of If1 on F_1F_0-ATP synthase stability compared to Stf1 was also observed on purified mitochondria where we confirmed that the isolated loss of If1 was sufficient to almost completely abolish the pH-dependent inhibition of F_1F_0-ATP synthase (Figure S3A). As expected, F_1F_0-ATP synthase dimers deficiency drastically impaired *atp18*Δ growth on medium containing glycerol (2%) a non-fermentable carbon source (Figure 3F). Interestingly, the combined loss of the inhibitory peptides, which drastically reduced the level of the free F1

subcomplex, severely hampered the growth of *atp18*Δ mutant on glycerol (Figure 3F and G).

If1/Stf1 mitigate the impact of mitochondrial depolarizing stress on glycerol medium.

To further evaluate the metabolic importance of If1/Stf1, we took advantage of the great metabolic flexibility of *S. cerevisiae* and characterized the phenotype of the *inh1*Δ *stf1*Δ strain grown under various carbon sources. To this end, we compared different carbon sources promoting respiro-fermentative (glucose 0.5% or galactose 2%) and non-fermentative conditions (glycerol 2% or lactate 2%). The respective capacity to metabolize these carbon sources and produce biomass were assessed using drop tests and growth curves (Figures 4A and B). In parallel, the cellular respiration of yeast grown on different carbon sources was recorded using high-resolution respirometer O2K oxygraph under endogenous conditions; or in presence of ethanol alleviating potential kinetic controls under endogenous, non-phosphorylating (triethyltin (TET)) and uncoupled (CCCP titration) states (Figure 4C). These combined approaches assessing the growth of the *inh1*Δ *stf1*Δ strain in various metabolic conditions demonstrated that the loss of the inhibitory peptides did not affect growth (Figure 4 A and B). The cellular respiration assessed during exponential phase demonstrated that OXPHOS capacities are strongly adjusted in response to the carbon sources. As expected, the overall respiration rates as well as the part of the respiration devoted to ATP synthesis (respiration loss in response to triethyltin), were low in the highly glycolytic glucose medium, intermediate in galactose and glycerol and high in the highly oxidative lactate medium. Interestingly, the *inh1*Δ *stf1*Δ strain grown under galactose, glycerol or lactate, consistently exhibited a significantly higher respiration compared to the WT strain. These results indicate that the combined loss of If1/Stf1 is linked to an increased OXPHOS activity (Figure 4C).

The enhanced OXPHOS activity of the *inh1*Δ *stf1*Δ strain prompted us to evaluate its capacity to respond to OXPHOS uncoupling stress induced by the mitochondrial depolarizing agent CCCP. To this end, yeast cultures were supplemented with the minimal CCCP concentration abolishing cellular respiration responses to triethyltin or CCCP validating that mitochondria are fully uncoupled (Figure 4C). The CCCP treatment did not affect the growth of the *inh1*Δ *stf1*Δ or WT strains under fermentable carbon sources as glucose (0.5%) or galactose (2%) (Figure 4A and B). However, the CCCP treatment differentially impacted the growth of the two strains under non fermentable carbon sources *i.e.* glycerol (2%) or lactate (2%) (Figure 4A and B). The mitochondrial uncoupling stress, under lactate (2%) medium, almost completely prevented the growth of both strains

(Figure 4A and B) causing severe deficiency of cellular respiration (Figure 4C). In contrast, the *inh1*Δ *stf1*Δ and WT strains cultivated under glycerol (2%) strongly differ in their ability to tolerate the uncoupling stress (Figure 4A and B). Our analyses clearly demonstrate that the If1/Stf1 inhibitors are essential to mitigate the impact of OXPHOS uncoupling stress on cell growth (Figure 4A, B and S4A) and respiration (Figure 4C).

Glycerol is a glyco-oxidative metabolic condition where the energy balance relies on ATP production from both glycolysis and OXPHOS.

To further investigate the If1/Stf1 mediated mechanism involved in the OXPHOS uncoupling stress response, we first quantified If1 and Stf1 levels in different growth conditions. Western blot analyses performed on total protein extracts from WT yeast grown under various carbon sources demonstrated that the levels of both If1 and Stf1 normalized to the F_1F_0-ATP synthase subunit β, were almost doubled under the different non-fermentable conditions compared to glucose or galactose conditions (Figure 5A and B). Our results also showed that the increased levels of both inhibitors in glycerol and lactate were not associated with specific changes in the free F_1 subcomplex (Figure S5A). Also, the levels of If1 and Stf1 were not impacted during the OXPHOS uncoupling stress (Figure S5B). The uniform expression of If1 and Stf1 under lactate and glycerol conditions indicated that the WT strain's resistance toward uncoupling stress in glycerol media was not merely due to changes in If1/Stf1 expression levels (Figure 5A and B). We then decided to challenge the assumed metabolic homogeneity between glycerol or lactate conditions, commonly defined as non-fermentable carbon sources relying on OXPHOS activity. To determine the dependency of energy toward the OXPHOS or glycolytic produced ATP, we followed the growth of genetically engineered yeast mutants presenting altered glycolysis or OXPHOS driven ATP production (Figure 5C). The previously generated and characterized mutant yeast strains *cdc19*Δ and *atp18*Δ (Sprague, 1977; Vaillier et al., 1999), respectively suppressed of pyruvate kinase 1 and subunit i/j of ATP synthase protein. This mutants were selected to decipher the growth dependency toward these different energy producing pathways. The drop test analyses performed with these 2 strains (Figure 5C) and other mutants abolishing the ATP synthase assembly and activity (Figure S5C-F), nicely confirmed that the growth on glucose or galactose media almost exclusively relied on the glycolysis-driven ATP production (insensitive to OXPHOS ATP production defects). Conversely, the growth on lactate medium almost exclusively relied on the OXPHOS-driven ATP production (insensitive to defective glycolytic ATP production) (Figure 5C and S5C-E). However, the drop test experiment unexpectedly demonstrated that the growth on glycerol medium is hindered either by defects in OXPHOS or glycolysis-

driven ATP production (Figure 5C and S5C-E). This strongly confirms the ability of glycerol metabolism by-products such as glycerol-3-phosphate (G3P) and dihydroxyacetone phosphate (DHAP) to fuel both OXPHOS from Gut2p and glycolysis from the triose phosphate intermediates (Figure 5D).

To further investigate the metabolic importance of the alternative glycolytic-driven ATP production in response to uncoupling stress, we measured, using HPIC method, the adenylic energy charge of *inh1*Δ *stf1*Δ and WT strains cultivated under glycerol medium (Figure 5E). The adenylate energy charge measurement demonstrated that, in the WT strain, the glycolytic-driven ATP production pathway could preserve the cells' energy status from OXPHOS uncoupling stress. The fact that adverse energetic outcomes associated with the loss of If1/Stf1 only appeared under depolarization stress strongly suggests that the drop in adenylate energy charge is caused by the un-prevented ATP hydrolysis from the reversed mitochondrial F_1F_0-ATP synthase assemblies. Further analyses demonstrated that this acute energy crisis occurring within the first hour of treatment (Figure 5E), affected cellular respiration at later time points (Figure 4C). Interestingly, the respiration defects were associated with decreased levels and activities of complex III, IV and V (Figure 5F and G), but the OXPHOS deficiencies were not linked to mitochondrial genome deficiency (Figure 5H) or loss of complex IV subunits (Figure 5I). Altogether, our analyses demonstrate that the canonical role of If1/Stf1 in preventing ATP hydrolysis and safeguarding energy metabolism under mitochondrial depolarization stress is unmasked under the very specific glyco-oxidative metabolic condition *i.e.* where yeast energy metabolism relies both on glycolysis and OXPHOS activities.

The If1/Stf1 inhibitors as well as F_1F_0-ATP synthase free F_1 subcomplex are both dispensable for the viability of $\rho^{-/\circ}$ yeasts

According to several reports, the ATPase activity of the free F_1 subcomplex coupled to the electrogenic activity of the adenine nucleotide translocator (ANT), is crucial to support mitochondrial membrane potential and growth of yeast lacking their mitochondrial genome ($\rho^{-/\circ}$ cells) (Clark-Walker, 2007; Giraud and Velours, 1997; Kominsky et al., 2002). The improved growth capacity of $\rho^{-/\circ}$ cells lacking If1 also strongly endorsed the importance of the free F_1 subcomplex ATPase activity in supporting the growth of mtDNA deprived cells (Liu et al., 2021). These previous works supporting that free F_1 subcomplexes could be more active in the absence of If1 in the context of $\rho^{-/\circ}$, would contrast with the interdependence between If1/Stf1 and free F_1 subcomplex we observed (Figure 1 and 2). Therefore, we decided to characterize the interplay between If1/Stf1 and free F_1 subcomplex in the context of $\rho^{-/\circ}$ cells. First, during the stationary growth phase of WT and

*inh1*Δ *stf1*Δ, we analyzed the proportion of cells undergoing $\rho^{-/\circ}$ conversion. In line with previous works, we observed that the loss of If1/Stf1 activity was in fact favoring the loss of mitochondrial genome and the conversion of yeast into $\rho^{-/\circ}$cells (Figure 6A). Then, we generated stable WT and *inh1*Δ *stf1*Δ $\rho^{-/\circ}$ cells and observed that the If1/β ratio was unchanged in WT $\rho^{-/\circ}$ whereas the Stf1/β ratio, while not significant, tended to be reduced (Figure 6B). While favoring the conversion into $\rho^{-/\circ}$ cells (Figure 6A), the loss of If1/Stf1 did not impact the $\rho^{-/\circ}$ cells' growth rate under fermentative conditions (Figure 6C). Moreover, our data demonstrated that the overall ATP hydrolysis activity (Figure 6D) as well as the free F_1 subcomplex expression (Figure 6E) were barely detected in total extracts from WT and *inh1*Δ *stf1*Δ $\rho^{-/\circ}$ cells. Interestingly, BN-PAGE experiments performed on highly concentrated extracts from $\rho^{-/\circ}$ cells confirmed that the free F_1 subcomplex levels were, like in the ρ^{+} context (Figure 1D), severely reduced in the *inh1*Δ *stf1*Δ $\rho^{-/\circ}$ compared to the WT $\rho^{-/\circ}$ cells. Collectively, our findings suggest that the deletion of If1/Stf1 is beneficial for $\rho^{-/\circ}$ cells, but they also refute hypotheses supporting that this effect could be tightly linked to an activation of the F_1 subcomplex driven ATP hydrolysis. Instead, our results demonstrated that the loss of If1/Stf1 together with the free F_1 subcomplex favored the conversion into $\rho^{-/\circ}$ and did not affect the growth of $\rho^{-/\circ}$ cells on fermentable carbon sources (Figure 6).

Discussion

The present work confirmed that, in contrast to their mammalian homologs If1, the yeast If1/Stf1 inhibitors are dispensable for the biogenesis and stability of F_1F_0-ATP synthase dimers and provides first evidence that If1/Stf1 are not required for the stability of F_1F_0-ATP synthase oligomers. The resolution of the F_1F_0-ATP synthase tetramers' structures by Cryo-EM, demonstrating that If1 dimers could bridge and likely stabilize adjacent dimers (Gu et al., 2019; Pinke et al., 2020; Mühleip et al., 2021), has supported the previously proposed role of If1 in the supramolecular organization of the mammalian F_1F_0-ATP synthase (Cabezón et al., 2000). The role of mammalian If1 in F_1F_0-ATP synthase supramolecular organization was recently strengthened, by single molecule tracking microscopy and native electrophoresis performed on If1 knock-in and knock-out cell lines (Romero-Carramiñana et al., 2023; Weissert et al., 2021). In contrast, the lack of cryo-EM structures of yeast F_1F_0-ATP synthase oligomers larger than dimers (Hahn et al., 2016), along with previously characterized differences in If1 dimerization and function, has cast doubts on the potential implication of If1/Stf1 inhibitors in the F_1F_0-ATP synthase

supramolecular organization in yeast (Cabezon et al., 2002; Hong and Pedersen, 2002; Le Breton et al., 2016). Our work confirms previous findings showing that the levels of F_1F_0-ATP synthase dimers remained unchanged in *inh1*Δ *stf1*Δ (Dienhart et al., 2002), but also demonstrates that loss of these inhibitory peptides does not preclude the assembly and levels of higher molecular weight F_1F_0-ATP synthase oligomers (Figure 1C). Instead, structural and functional investigations consistently demonstrated that If1 is required to maintain the levels of the free F_1 subcomplex, which is functionally characterized by its oligomycin insensitivity (Figure 1 and 2) (Wittig et al., 2007). Our findings also support previous works demonstrating that ATP synthase dimers can form rows and induce membrane curvature just from the intrinsic shape of the dimer without the need for If1 connecting neighbouring dimers together (Davies et al., 2012; Anselmi et al., 2018; Blum et al., 2019).

The free F_1 subcomplex observed under native PAGE or density gradients used to be considered as an artifact resulting from the destabilization of fully assembled F_1F_0-ATP synthase (monomers and oligomers) by the action of detergent or improper sample preparation and storage (Ackerman and Tzagoloff, 1990; Jänsch et al., 1996; Wittig et al., 2007). The native PAGE and solubilization techniques development combined with the use of milder detergents such as digitonin have since convincingly demonstrated that the free F_1 subcomplexes were stable assembly intermediates formed independently from the ATP synthase F_0 sectors (Li et al., 2012; Nijtmans et al., 1995). The native PAGE and oligomycin-sensitive enzymatic analyses, have independently demonstrated that the ratio between the free F_1 subcomplex and the fully assembled F_1F_0-ATP synthase was impacted neither by the use of mild detergent nor by the BN-PAGE approach. Our findings support that the free F_1 subcomplex is not a degradation by-product resulting from digitonin treatment since no F_1 subcomplex could be detected in the digitonin-solubilized membrane fraction containing fully assembled F_1F_0-ATP synthases (Figure 1C-E). Instead, our work strongly supports previous reports claiming that the free F_1 subcomplex is a stable intermediate assembly. This hypothesis is also strengthened by the enhanced levels of free F_1 we observed in yeast presenting aberrant ATP synthase assembly such as *atp18*Δ (Figure 3C) and $\rho^{-/\circ}$ (Figure 6E and F), corroborating independent observations obtained in different model organisms (Carrozzo et al., 2006; Wittig et al., 2006, 2007; Mourier et al., 2014; He et al., 2018). Our quantitative analyses substantiate independent reports demonstrating that If1 binding affinity and inhibitory capacities are greater than Stf1 (Cabezon et al., 2002; Venard et al., 2003). Interestingly, we demonstrated that If1 evenly

binds the various ATP synthase assemblies (Figure 2A and B) and can very efficiently inhibit their ATP hydrolysis activity in a characteristic pH-dependent manner (Figure 2C-E).

Several independent studies have previously demonstrated that the maintenance of mitochondrial membrane potential and the ADP/ATP translocator were essential for the survival and growth of yeast presenting long range deletion (ρ^-) or complete loss of their mitochondrial genome ($\rho°$) (Dupont et al., 1985; Kovácová et al., 1968; Subík et al., 1972). This specific sensitivity prompted scientists to hypothesize that the F_1 subcomplex driven ATP hydrolysis together with the electrogenic activity of the ADP/ATP translocator could be key in maintaining the proton electrochemical potential across the mitochondrial inner membrane and therefore essential for the growth and survival of $\rho^-/°$ yeast (Giraud and Velours, 1997; Chen and Clark-Walker, 1999; Clark-Walker, 2007). Our analyses demonstrated that the loss of If1/Stf1 associated with drastic loss of F_1 subcomplex does not prevent the yeast to undergo $\rho^-/°$ conditions nor impact their growth under fermentative carbon source (Figure 6). Consequently, our results corroborate original analyses from Tzagaloff and Schatz (Tzagoloff et al., 1975) demonstrating that the loss of subunits forming the F_1 sector did not preclude the conversion into $\rho^{-/°}$ cells.

For endogenous peptide inhibitors, the free F_1 subcomplex is a priority target because of its potential toxicity for the cell's energy metabolism. In contrast to the fully assembled F_1F_0-ATP synthase, the toxicity of the free F_1 subcomplex stems from its lack of thermodynamic feedback inhibition by the proton electrochemical potential. The novel fIf1/Stf1-mediated mechanism of action identified in the present work, elegantly circumvents any potentially uncontrolled ATP hydrolysis from the yeast free F_1 subcomplex. Our present work demonstrates that in the presence of If1/Stf1 the free F_1 subcomplex is tightly regulated and inhibited, whereas in the absence of If1 the free F_1 subcomplex is not maintained (Figure 1 and 2). Altogether, our data suggest that the If1 binding to the free F_1 subcomplex is not only preventing potential toxic ATP hydrolysis, but also stabilizing this assembly intermediate (Figure 3A). This peculiar interplay between If1 and the yeast free F_1 subcomplex is in agreement with the parallel increase in If1 and ATP synthase subassemblies we previously characterized in cardiac-specific knockouts developing a progressive cardiomyopathy associated with mitochondrial transcripts instability (Mourier et al., 2014).

Interestingly, the loss of If1/Stf1 inhibition on the fully assembled F_1F_0-ATP synthase was associated with a mild stress increasing cellular respiration capacity, but without affecting

the growth rate (Figure 4). However, the CCCP-induced OXPHOS uncoupling stress unmasks the crucial role played by If1/Stf1 under a very specific metabolic condition associated with the glycerol carbon source. The systematic comparison of cellular respiration of cells growing under fermentable (glucose 0.5%, galactose 2%) and non-fermentable (glycerol 2%, lactate 2%) carbon sources demonstrated that mitochondrial respiration alone was insufficient to comprehend the unique metabolic specificity of cells metabolizing glycerol (Figure 4). In contrast to the glucose or lactate conditions presenting striking differences in their respirations, it was impossible to discriminate, on the basis of their endogenous respiration, yeast grown on galactose (non-fermentable) or glycerol (fermentable) (Figure 4). This observation prompted us to develop a new screening tool using genetically modified yeast presenting defective mitochondrial or glycolytic-driven ATP production to decipher the respective implication of the two pathways in energy balance and yeast growth (Figure 5C). This strategy demonstrated that in contrast to lactate medium where yeast growth was exclusively dependent on the mitochondrial pathway, growth on glycerol also relied on the pyruvate kinase 1 (Cdc19) glycolysis activity. This observation demonstrated that glycerol, in contrast to lactate, is not a strict ‘non-fermentable’ carbon source strictly relying on mitochondrial energy metabolism. This observation corroborates recent hypotheses based on transcriptomic and metabolomic analyses and challenging the classification of glycerol as a ‘non-fermentable’ carbon source (Aßkamp et al., 2019; Galkina et al., 2022; Xiberras et al., 2019). Assessing the relative dependence of cell energy metabolism on glycolysis and oxidative phosphorylation was more pertinent for understanding the role of If1/Stf1 in OXPHOS uncoupling stress in glycerol, than simply characterizing metabolism through respiro-fermentative properties. Accordingly, the specific If1/Stf1 dependency of cells under glycerol, redefined here as a glyco-oxidative metabolic condition, suggests that preventing mitochondrial ATP hydrolysis is crucial for cell growth only when energy metabolism evenly relies on both glycolysis and OXPHOS processes (Figure 5 C-E). In contrast, the unrepressed ATPase activity did not affect cell growth on highly glycolytic conditions (glucose or galactose) and conversely could not be compensated under highly oxidative metabolic conditions (lactate). We believe that this new approach deciphering the respective roles of glycolysis and OXPHOS in cell energy balance applied to the mammalian context could help understand the intriguing role of If1 in numerous tumors undergoing hypoxic stress and overexpressing this inhibitory peptide (Sánchez-Aragó et al., 2013; Sgarbi et al., 2018).

_ Figure 1 _

If1/Stf1 are required to maintain the F_1F_0-ATP synthase free F_1 subcomplex levels.

(A) Western blot performed on total cell protein extracts purified from WT, *inh1*Δ, *stf1*Δ and *inh1*Δ *stf1*Δ mutants, grown on glycerol 2% rich medium. (Representative of n = 5 independent experiments)

(B) Growth of WT (black) and *inh1*Δ *stf1*Δ (red) mutants on lactate 2% rich medium, following the optical density of the culture at 550 nm. (n = 5 independent experiments).

(C) CN-PAGE (3-12%) performed with purified mitochondria from WT and *inh1*Δ *stf1*Δ cells grown on lactate 2% rich medium, solubilized with glyco-diosgenin (GDN) at a GDN to protein ratio of 0.5 g/g protein. The F_1F_0-ATP synthase assemblies were revealed by F_1F_0-ATP synthase hydrolytic in-gel activity (CV IGA). (Representative of n = 3 independent experiments)

(D) CN and BN-PAGE (3-12%) performed with total cell extracts from WT and *inh1*Δ *stf1*Δ grown on glycerol 2% rich medium solubilized with digitonin at a digitonin to protein ratio of 1.5 g/g protein. The F_1F_0-ATP synthase assemblies were revealed by F_1F_0-ATP synthase hydrolytic in-gel activity (CV IGA). (Representative of n = 3 independent experiments)

(E) CN and BN-PAGE (3-12%) performed with total cell extracts, membrane and soluble fractions obtained after ultracentrifugation of WT cells grown on glycerol 2% rich medium solubilized with digitonin at a digitonin to protein ratio of 1.5 g/g protein. The F_1F_0-ATP synthase assemblies were revealed by F_1F_0-ATP synthase hydrolytic in-gel activity (CV IGA). (Representative of n = 3 independent experiments)

(F) BN-PAGE (3-12%) performed with total cell extracts from WT, *inh1*Δ *stf1*Δ*, inh1*Δ and *stf1*Δ*,* grown on glycerol 2% medium solubilized with digitonin at a digitonin to protein ratio of 1.5 g/g protein. The F_1F_0-ATP synthase assemblies were revealed by F_1F_0-ATP synthase hydrolytic in-gel activity (CV IGA). (Representative of n = 3 independent experiments)

_ Figure 2 _

If1 binds and inhibits ATP synthase oligomers, monomers and free F_1 subcomplexes.

(A) Western blot following 2D-BN/SDS-PAGE performed with total cell extracts from WT and the *inh1*Δ *stf1*Δ grown on glycerol 2% rich medium. During the extraction and solubilization, the pH was conserved at 6.4 to preserve If1/Stf1 binding. (Representative of n = 3 independent experiments)

(B) Densitometric quantification of western blot following 2D-BN/SDS-PAGE performed with total cell extracts from WT cells grown on glycerol 2% rich medium. For each F_1F_0-ATP synthase assembly, the western blot signal obtained with If1 signal was normalized to the β or γ subunit.

(C) Measurement of the ATP hydrolysis flux performed on total cell extracts from WT (black bars) and *inh1*Δ *stf1*Δ (red bars) grown on glycerol 2% rich medium by monitoring the ATP induced phosphate production over several minutes. Experiments were performed at pH 9.0 (inactive inhibitors) and pH 6.4 (active inhibitors). (n = 3 independent experiments, unpaired t-test, error bars ± SEM **p<0.005)

(D) Measurement of the ATP hydrolysis flux performed on total cell extracts from WT (black bars) and *inh1*Δ *stf1*Δ (red bars) grown on glycerol 2% rich medium by monitoring the ATP induced phosphate production over several minutes. Experiments were performed at pH 9.0 (inactive inhibitors) in absence or presence of oligomycin. (n = 3 independent experiments, unpaired t-test, error bars ± SEM *p<0.05)

(E) Measurement of the ATP hydrolysis flux performed on the soluble fraction purified from total cell extracts from WT (black bars) and *inh1*Δ *stf1*Δ (red bars) grown on glycerol 2% rich medium by monitoring the ATP induced phosphate production over several minutes. Experiments were performed at pH 9.0 (inactive inhibitors) and pH 6.4 (active inhibitors), in absence or presence of oligomycin. (n = 3 independent experiments, unpaired t-test, error bars ± SEM)

_ Figure 3 _

If1 and Stf1 are specifically involved in free F_1 subcomplex stabilization.

(A) BN-PAGE (3-12%) performed with total cell extracts, from WT and *inh1*Δ *stf1*Δ grown on glycerol 2% rich medium subjected to cycloheximide (250 µg/ml) during 0, 30 and 90 minutes. Samples were solubilized with digitonin at a digitonin to protein ratio of 1.5 g/g protein. The F_1F_0-ATP synthase assemblies were revealed by F_1F_0-ATP synthase hydrolytic in-gel activity (CV IGA). (Representative of n = 3 independent experiments)

(B) Western blot (left) and densitometric analysis (right) of the relative abundance of IF1 (black) and STF1 (grey) from total cell extracts from WT grown on glycerol 2% rich medium subjected to cycloheximide (250 µg/ml) during 0, 30 and 90 minutes. Densitometric signals were normalized to the t_0-condition without cycloheximide. The ponceau staining as well as the Coomassie blue staining presented in the upper part demonstrate (i) that samples are evenly loaded and (ii) that the tagged If1 and Stf1 produced *in vitro* and used for relative quantification levels are equally loaded in the standard. (n = 3 independent experiments, 2-way ANOVA, error bars ± SEM)

(C) CN and BN-PAGE (3-12%) performed with total cell extracts, from WT, *inh1*Δ *stf1*Δ, *atp18*Δ and *atp18*Δ *inh1*Δ cells grown on glycerol 2% rich medium solubilized with digitonin at a digitonin to protein ratio of 1.5 g/g protein. The F_1F_0-ATP synthase assemblies were revealed by F_1F_0-ATP synthase hydrolytic in-gel activity (CV IGA). (Representative of n = 4 independent experiments)

(D) BN-PAGE (3-12%) performed with total cell extracts, from WT, *atp18*Δ*, atp18*Δ *inh1*Δ *stf1*Δ*, atp18*Δ *inh1*Δ and *atp18*Δ *stf1*Δ grown on glycerol 2% rich medium solubilized with digitonin at a digitonin to protein ratio of 1.5 g/g protein. The F_1F_0-ATP synthase assemblies were revealed by F_1F_0-ATP synthase hydrolytic in-gel activity (CV IGA). (Representative of n = 3 independent experiments)

(E) Growth of WT (black circles), *atp18*Δ (orange circles), *atp18*Δ *inh1*Δ (brown circles) and *atp18*Δ *inh1*Δ *stf1*Δ (purple circles) on glycerol 2% rich medium, following the optical density of the culture at 550 nm. (n = 3 independent experiments)

(F) Drop test performed on WT, *atp18Δ, atp18Δ stf1Δ, atp18Δ inh1Δ* and *atp18Δ inh1Δ stf1Δ* grown on glycerol 2% rich medium. (Representative of n = 3 independent experiments)

_ Figure 4 _

If1/Stf1 mitigate the impact of mitochondrial depolarizing stress on glycerol medium.

(A) Drop test performed on WT and *inh1*Δ *stf1*Δ grown on different fermentable (glucose 0.5%, galactose 2%) and non-fermentable (glycerol 2%, lactate 2%) culture rich media supplemented or not with CCCP (Representative of n = 3 independent experiments)

(B) Growth of WT (black circles and black crosses when supplemented with CCCP), and *inh1*Δ *stf1*Δ (red circles and red crosses when supplemented with CCCP) cells on different fermentable (glucose 0.5%, galactose 2%) and non-fermentable (glycerol 2%, lactate 2%) culture rich media supplemented (crosses) or not with CCCP (circles), following the optical density of the culture at 550 nm. (n = 3 independent experiments)

(C) High resolution respirometry performed on WT (black bars and hatched black bars in presence of CCCP) and *inh1*Δ *stf1*Δ cells (red bars and hatched red bars in presence of CCCP), collected during exponential phase on different fermentable (glucose 0.5%, galactose 2%) and non-fermentable (glycerol 2%, lactate 2%) culture rich media, supplemented (hatched bars) or not (empty bars) with CCCP (9h incubation). The oxygen consumption fluxes were normalized to optical density. Cellular respiration was measured under endogenous state and in the presence of ethanol, under endogenous, non-

phosphorylating (triethyltin titration) and uncoupled (CCCP titration) states. (n ≥ 3 independent experiments, two-way ANOVA, error bars ± SEM *p<0.05, **p<0.005, ***p<0.0005)

_ Figure 5 _

F_1F_0-ATP synthase peptide inhibitors activity is crucial to preserve energy metabolism under glyco-oxidative metabolism.

(A) Western blot and (B) densitometric analysis of the relative abundance of If1 and Stf1 in regard to the F_1F_0-ATP synthase β subunit level. Denaturing electrophoresis was performed using total cell extracts from WT grown on different fermentable (glucose 0.5%, galactose 2%) and non-fermentable (glycerol 2%, lactate 2%) culture rich media. Densitometric signals were normalized to the glycerol condition. The ponceau staining as well as the Coomassie blue staining presented in the upper part demonstrate (i) that samples are evenly loaded and (ii) that the tagged If1 and Stf1 produced *in vitro* and used for relative quantification levels are equally loaded in the standard. (n = 8 independent experiments, two-way ANOVA, error bars ± SEM *p<0.05, **p<0.005).

(C) Drop test performed on WT, *cdc19Δ* thermosensitive (*ts*) mutant (37°) and *atp18Δ* mutant grown on different fermentable (glucose 0.5%, galactose 2%) and non-fermentable (glycerol 2%, lactate 2%) culture minimum media. (Representative of n = 3 independent experiments)

(D) Scheme of the main metabolic pathways involved in ATP/ADP maintenance characterizing the so-called glyco-oxidative metabolism observed under glycerol 2% conditions.

(E) HPIC quantification of adenylate energy charge in WT (black) and *inh1*Δ *stf1*Δ (red) cells grown in the absence (circles) or presence (crosses) of CCCP (1 h incubation) on glycerol 2% rich medium. (n = 3 independent experiments, one-way ANOVA, Error bars ± SEM ***p<0.0005)

(F) BN-PAGE (3-12%) performed with total cell extracts from WT and *inh1*Δ *stf1*Δ grown on glycerol 2% rich medium solubilized with digitonin at a digitonin to protein ratio of 1.5 g/g protein. NADH dehydrogenase, complex IV (CIV) and F_1F_0-ATP synthase (CV) in-gel activities (IGA) were performed. (Representative of n = 3 independent experiments)

(G) Enzymatic activity of the respiratory chain complex III (CIII) performed on total cell extracts from WT and *inh1*Δ *stf1*Δ cultivated on glycerol 2% rich medium, in the presence or absence of CCCP (6h incubation). All the fluxes were normalized to WT condition without CCCP. (n ≥ 9 independent experiments, error bars ± SEM (**p<0.005))

(H) Quantitative PCR quantification of the mitochondrial DNA to nuclear DNA ratio performed on total DNA extracted from WT and *inh1*Δ *stf1*Δ grown on glycerol 2%, in the presence (hatched bars) or absence (solid bars) of CCCP (6 h incubation). (n = 3 independent experiments, 2-way ANOVA, error bars ± SEM)

(I) Western blot (left) and densitometric (right) analysis of the relative abundance of Cox2, a complex IV subunit. Denaturing electrophoresis was performed using total cell extracts from WT and *inh1*Δ *stf1*Δ grown on glycerol 2% rich medium in the presence or absence of CCCP (6h incubation). Immunodetected signals were normalized to ponceau signal. (n = 3 independent experiments, one-way ANOVA, error bars ± SEM)

_ Figure 6 _

The If1/Stf1 inhibitors as well as F_1F_0-ATP synthase free F_1 subcomplex are both dispensable for the viability of $\rho^-/°$ yeast

(A) Percentage of WT and *inh1*Δ *stf1*Δ cells that spontaneously lost their mitochondrial genome $\rho^-/°$. (n = 8 independent experiments, unpaired t-test, error bars ± SEM ***p<0.0005)

(B) Western blot (left) and densitometric analysis (right) of the relative abundance of If1 and Stf1 in regards to the F_1F_0-ATP synthase β subunit level. Denaturing electrophoresis was performed on total cell extracts from WT (black) and WT $\rho^-/°$ (grey) grown on glucose 0.5% rich medium. (n = 3 independent experiments, unpaired t-test, error bars ± SEM *p<0.05)

(C) Growth of WT (black circles) or WT $\rho^-/°$ (black triangles), *inh1*Δ *stf1*Δ (red circles) and *inh1*Δ *stf1*Δ $\rho^-/°$ (red triangles) cell on glucose 0.5% rich medium, following the optical density of the culture at 550 nm. (n = 3 independent experiments)

(D) Measurement of the ATP hydrolysis flux performed on total cell extracts from WT (black bars) and *inh1*Δ *stf1*Δ (red bars) and their $\rho^-/°$ variants, grown on glucose 0.5% rich medium by monitoring the ATP induced phosphate production over several minutes. Experiments were performed at pH 9.0 (inactive inhibitors). (n = 3 independent experiments, unpaired t-test, error bars ± SEM **p<0.005)

(E) BN-PAGE (3-12%) performed with total cell extracts from WT and *inh1*Δ *stf1*Δ and their respective $\rho^-/°$- variants, grown on glucose 0.5% rich medium. Cell extracts were solubilized with digitonin at a digitonin to protein ratio of 1.5 g/g protein. NADH dehydrogenase and F_1F_0-ATP synthase (CV) in-gel activities (IGA) were performed. (Representative of n = 3 independent experiments)

(F) BN-PAGE (3-12%) performed with highly concentrated total cell extracts from WT, WT $\rho^-/°$ and *inh1*Δ *stf1*Δ $\rho^-/°$ grown on glucose 0.5% rich medium. Cell extracts were

solubilized with digitonin at a digitonin to protein ratio of 1.5 g/g protein. The F_1F_0-ATP synthase assemblies were revealed by ATP synthase hydrolytic in-gel activity (CV IGA). (Representative of n = 3 independent experiments)

SUPPLEMENTAL

Supplemental Figure 1

BN-PAGE (3-12%) (A) and densitometric analysis (B) performed with total cell extracts, from WT, *inh1*Δ *stf1*Δ *and atp18*Δ grown under glycerol 2% rich medium. Cell extracts were solubilized with increasing digitonin to protein ratio ranging from 0.5 to 6 g/g protein. The ATP synthase assemblies (O: oligomers; V: monomers; F_1: free F_1 subcomplex) were revealed by F_1F_0-ATP synthase (CV) hydrolytic in-gel activity (IGA). (n = 4, two-way ANOVA, error bars ± SEM *p<0.05)

Supplemental Figure 3

(A) Measurement of the ATP hydrolysis flux performed on purified mitochondria from total cell extracts from WT (black bars) and *inh1*Δ (red bars) grown on lactate 2% rich medium by monitoring the ATP induced phosphate production flux over several minutes. Experiments were performed at pH 9.0 (inactive inhibitors) and pH 6.4 (active inhibitors). (n ≥ 7 independent experiments, unpaired t-test, error bars ± SEM ***p<0.0005)

Supplemental Figure 4

(A) Determination of doubling time (hours) of WT (black bars) and *inh1Δ stf1Δ (red bars)* grown on different fermentable (glucose 0.5%, galactose 2%) and non-fermentable (glycerol 2%, lactate 2%) culture rich media supplemented or not with CCCP (1, 1.5 or 2 µM), following the optical density of the culture at 550 nm. *nd*: not determined *i.e* too slow to determine the doubling time (n = 3 independent experiments, two-way ANOVA, error bars ± SEM)

Supplemental Figure 5

(A) BN-PAGE (3-12%) performed with total cell extracts from WT grown on different fermentable (glucose 0.5%, galactose 2%) and non-fermentable (glycerol 2%, lactate 2%) culture rich media. Cell extracts were solubilized with digitonin at a digitonin to protein ratio of 1.5 g/g protein. 150 µg of protein were loaded for glucose or galactose condition and 100 µg of protein were loaded for glycerol or lactate conditions. The F_1F_0-ATP synthase

assemblies were revealed by F_1F_0-ATP synthase (CV) hydrolytic in-gel activity (IGA). (Representative of n = 2 independent experiments)

(B) Western blot (left) and densitometric analysis (right) of the relative abundance of If1 and Stf1, using Pgk1 as loading control. Denaturing electrophoresis was performed with total cell extracts grown on glycerol 2% rich medium supplemented or not with CCCP. The Coomassie blue staining on the upper panel demonstrates the equal loading of tagged If1 and Stf1 produced *in vitro* and used for the relative quantification of inhibitors (* signal remaining from anti-STF1 antibody). (n = 3 independent experiments, unpaired t-test, error bars ± SEM)

(C) Densitometric analysis of drop test performed on WT (black) and *atp18Δ* (orange) mutant grown on glycerol 2% culture minimum medium. (n = 3 independent experiments, two-way ANOVA, error bars ± SEM)

(D) Densitometric analysis of drop test performed on WT (black) and *cdc19Δ (green)* thermosensitive (*ts*) mutant (37°) mutant grown on glycerol 2% culture minimum medium. (n = 3 independent experiments, two-way ANOVA, error bars ± SEM)

(E) Densitometric analysis of drop test performed on WT (black) and *cdc19Δ (green)* thermosensitive (*ts*) mutant (37°) mutant grown on lactate 2% culture minimum medium. (n = 3 independent experiments, two-way ANOVA, error bars ± SEM)

(F) Drop test performed on WT, *atp5Δ, atp7Δ and atp14Δ* mutant grown on different fermentable (glucose 0.5%, galactose 2%) or non-fermentable (glycerol 2%, lactate 2%) culture minimum media. (Representative of n = 3 independent experiments)

Mat & meth

Yeast strains

The *Saccharomyces cerevisiae* strain used in this study is the strain D273-10B/A/H/U (MAT α, met6, ura3, his3) referred to as the wild type (WT)(Paul et al., 1989) and strain BY4741 Euroscarf (*MAT α; his3Δ1; leu2Δ0; met15Δ0; ura3Δ0*). The mutants D273 were obtained by homologous recombination of the following deletion cassette in the wild type strain: D273 *inh1Δ* (*MAT α, met6, ura3, his3, inh1::HIS3-kanMX6),* D273 *stf1Δ* (*MAT α, met6, ura3, his3, stf1::Nat*^{R}), D273 *inh1Δ stf1Δ* (*MAT α, met6, ura3, his3, stf1::Nat*^{R}*, inh1::HIS3-KanMX6*), D273 *atp18Δ* (*MAT α, met6, ura3, his3, atp18::HIS3*), D273 *atp18Δ inh1Δ* (*MAT α, met6, ura3, his3, atp18::Nat*^{R}*, inh1::HIS3-kanMX6*), D273 *atp18Δ stf1Δ* (*MAT α, met6, ura3, his3, atp18::HIS3-kanMX6, stf1::Nat*^{R}), D273 *atp18Δ inh1Δ stf1Δ* (*MAT α, met6, ura3, his3, atp18::NatR, inh1::HIS3-kanMX6, stf1::Kan*^{R}). The plasmids used for the cassette *HIS3-kan*MX6 and nourseothricin resistance (*Nat*^{R}) were pFA6a-*His3*MX6 and pUG-natNT2 respectively. The generated mutants were validated by PCR and Western blot. D273 $\rho^{-/\circ}$ strain was obtained after growing cells on rich medium containing glucose 2% for two days before spreading on rich medium with 0.5% of glucose. The $\rho^{-/\circ}$ colonies were identified and counted by comparing to a replica plate containing glycerol rich medium where only the ρ^+ colonies were able to grow. The wild type and mutants strains BY4741 (*MAT a; his3Δ1; leu2Δ0; met15Δ0; ura3Δ0),* BY4742 (*MATα, lys2Δ0, ura3Δ0, his3Δ1, leu2Δ0*) and BY4743 (*MATa/MATα; his3Δ1/his3Δ1; leu2Δ0/leu2Δ0; LYS2/lys2Δ0; met15Δ0/MET15; ura3Δ0/ura3Δ0*) were provided by Euroscarf: BY4741 *atp18*Δ (*MAT a; his3Δ1; leu2Δ0; met15Δ0; ura3Δ0; YML081c-a::kanMX4*), BY4741 *cdc19*Δ (*MAT a; his3Δ1; leu2Δ0; met15Δ0; ura3Δ0; cdc19-1::kanMX4* (lethal at 37°C on glucose medium)), BY4742 *atp5Δ* (*MATα, lys2Δ0, ura3Δ0, his3Δ1, leu2Δ0, atp5::KAN*^{R}), BY4742 *atp7Δ* (*MATα, lys2Δ0, ura3Δ0, his3Δ1, leu2Δ0, atp7::KAN*^{R}), BY4742 *atp14Δ* (*MATα, lys2Δ0, ura3Δ0, his3Δ1, leu2Δ0, atp14::KAN*^{R}).

Yeast growth and media

Cells were grown aerobically at 28°C with shaking at 180 rpm. Growth was followed by measuring the optical density at 550 nm using a Jasco V-760 spectrophotometer. The composition of rich medium was: 0.1% (w/v) KH_2PO_4 pH 5.5, 1% (w/v) yeast extract, 0.12% (w/v) $(NH_4)_2SO_4$, 2% or 0.5% (w/v) carbon source and for solid medium 2% (w/v) bacto agar was added. For some drop test, cells were grown in the following minimum medium: 0.1% (w/v) KH_2PO_4 pH 5.5, 0.175% (w/v) yeast nitrogen base w/o amino acids and ammonium sulfate, 0.5% (w/v) $(NH_4)_2SO_4$, 0.2% (w/v), 2% or 0.5% (w/v) carbon source, 2% (w/v) bacto

agar minimum medium, 0.2% (w/v) casein hydrolysate, 100 mg/l leucine, 20 mg/l histidine, 20 mg/l methionine, 20 mg/l uracil. A filtered solution of casein and amino acids was added to the sterilized medium. Different carbon sources were used: D,L-lactic acid, glycerol, D(+)-galactose or D(+)-glucose. The carbon source and the type of medium (rich or minimum) selected for each experiment is indicated in the legends. The uncoupler agent CCCP was added in the liquid culture medium, at 28°C, a few minutes before inoculating the cells at 0.1 OD_{550nm} for growth curves and at 1 OD_{550nm} for HPIC experiments. For solid culture medium CCCP was added in the tepid medium just before solidification of agar and used within one day. A CCCP concentration titration (between 1.25 and 7.5 µM) was performed for each experiment and condition. The inhibitor of cytosolic translation, cycloheximide (250 µg/ml) was added in the culture medium, at 2 OD_{550nm} culture. Cells were harvested during exponential growth.

Mitochondria preparation

Yeast cells grown in the presence of 2% (w/v) lactate were collected during the exponential growth phase and mitochondria were prepared by enzymatic digestion of the cell wall with Zymolyase®-20T (nacalai tesque®, reference 07663-04) according to (Guérin et al., 1979).

High-resolution oxygen consumption measurement on yeast cells and isolated mitochondria.

Oxygen consumption of cells harvested during the exponential growth phase on different culture media was measured at 28°C using an Oxygraph-2k (OROBOROS INSTRUMENTS, Innsbruck, Austria). Oxygen consumption rates of cells were measured under endogenous state and in presence of 85 mM ethanol substrate under endogenous conditions, under the non-phosphorylating state with addition of 25 µM TET and under the uncoupled state by successive addition of CCCP titration (around 2.5 µM). When necessary, cells were diluted with the culture medium.

Protein extraction

100 units of OD_{550nm} were harvested, pelleted and washed with cold water before being broken by vigorous shaking for 4 min in 250 µl of extraction buffer containing 10 mM Bis-Tris-HCl pH 6.4, 1 mM EDTA and a mixture of protease inhibitors (Complete EDTA-free™, Roche) with an equal volume of glass beads (0.4 mm diameter). Protein concentrations were then determined using the DC assay according to manufacturer's instructions (Bio-Rad). To detect the free F_1 subcomplex in $\rho^{-/\circ}$, we obtained concentrated solubilized cell

protein extracts using a centrifugal Concentrator (Corning® Spin-X® UF 500 µL, molecular weight cut-off of 100 kDa). The supernatant was collected after centrifugation at 12,000g for 10 min at 4°C. To obtain the membrane and soluble fractions, the total cell extract was centrifuged at 30,000g during 30 min at 4°C. The supernatant (containing the soluble fraction) and pellet (containing the membrane fraction), were collected and subjected to protein quantification. The pellet was resuspended in a volume of extraction buffer equivalent to that of the harvested supernatant.

Enzymatic activities determination

Cytochrome c reductase (complex III) activity was determined by the absorbance at 550 nm of reduced cytochrome c in the following buffer: 50 mM KH_2PO_4 pH 7.4, 0.5 mM KCN, 10 mM succinate, 10 mM G3P and 200 µg/ml bovine heart cytochrome c. The specificity of the assay was validated by the addition of 0.5 µM antimycin A. Cytochrome c reductase (complex III) activity being defined as the antimycin A sensitive flux. Enzymatic activity measurements were performed with a Jasco V-760 spectrophotometer on 250 µg protein in a quartz spectrophotometer cell at 28°C with stirring at 1,000 rpm.

The hydrolytic activity of ATP synthase (complex V) was determined with 0.8 mg protein cell extracts at 28°C with shaking at 750 rpm with a thermomixer in the following buffer: 75 mM triethanolamine pH 9.0 or pH 6.4, 5 mM $MgCl_2$ with 2 µg/ml alamethicin. The reaction was initiated with the addition of 5 mM ATP andevery 2 min (or 6 min for ρ^-/°) an aliquot was collected and added to the following solution: 0.38 M sulfuric acid, 5 µM ammonium heptamolybdate tetrahydrate, 29 µM iron(II) sulfate heptahydrate. The Pi product was quantified following changes in the absorbance assessed at 750 nm. The same experiment was performed after a 2-min pre-incubation with 19 µg/ml oligomycin to assess the oligomycin-insensitive ATP hydrolysis flux. The hydrolytic activity of ATP synthase (complex V) on purified mitochondria (0.035 mg of mitochondrial protein) was determined at 28°C with shaking at 750 rpm in an Oroboros chamber in the following buffer: 75 mM triethanolamine pH 9.0 or 6.4, 5 mM $MgCl_2$ with 1 µg/ml alamethicin. The reaction was initiated with the addition of 5mM ATP. Every 30 s an aliquot was collected and added to the following solution: 0.38 M sulfuric acid, 5 µM ammonium heptamolybdate tetrahydrate, 29 µM iron(II) sulfate heptahydrate. The Pi product was quantified following changes in the absorbance assessed at 750 nm. The same experiment was performed after a 2 min pre-incubation with 4 ng/ml triethyltin to assess the oligomycin-insensitive ATP hydrolysis flux.

BN-PAGE analyses and two-dimensional electrophoresis on total yeast cells protein extracts

For CN and BN-PAGE, 100 or 200 µg of total cell protein extracts were solubilized with Glyco-diosgenin (GDN) (0.5g/g) or high-purity digitonin (1.5 g/g) in extraction buffer (see above) with 0.0125 kU/µl of nuclease. Membranes were solubilized by vortexing for 30 min at 4°C and incubated at room temperature for 10 min. Supernatants were collected after centrifugation of the solubilized protein extract at 30,000g for 30 min. The loading buffer containing 0.15 M 6-aminohexanoic acid was used for CN-PAGE and was supplemented with 20% (w/v) glycerol and 0.0125 % (w/v) Coomassie brilliant blue G-250 for BN-PAGE. Proteins samples were loaded on Bis-Tris Invitrogen™ Novex™ NativePAGE™ 3-12% acrylamide gradient gels. Gel migration was performed at 10 mA, 3 h at 4°C. At three-quarters of the migration, the BN-PAGE buffer was removed and replaced by a CN-PAGE buffer to decrease the blue coloration of gel.

Protein complexes were detected by in-gel activity as previously described (Molinié et al., 2022). Native gels were incubated with activity buffers containing 50 mM KH_2PO_4 pH 7.4 and 0.5 mg/ml iodonitrotetrazolium. The buffer was complemented with 400 µM NADH pH 7.0 to reveal NADH dehydrogenases. For cytochrome c reductase in-gel activity, native gels were incubated in the following buffer: 50 mM KH_2PO_4 pH 7.4, 75 mg/ml sucrose, 0.5 mg/ml 3,3'-Diaminobenzidine and 1 mg/ml cytochrome c. For ATP synthase in-gel activity, native gels were incubated in the following buffer: 50 mM glycine, 1.32 mM lead acetate, 0.1 % (w/v) Triton X-100, and supplemented with 5 mM $MgSO_4$ and 4 mM ATP pH 7.0 to start the reaction. After revelation of ATPase activity, native gels were incubated with 0.1% (v/v) HCl to remove lead precipitate before Coomassie staining (0.125% (w/v) Coomassie, 50% (v/v) ethanol, 10% (v/v) acetic acid). After 45 min, gels were destained with a destaining solution (25% (v/v) ethanol and 8% (v/v) acetic acid). After in-gel activity, Native gels were imaged using ImageQuant (Amersham) and the Optical Density was determined using FIJI analyzer.

For two-dimensional electrophoresis (2D-BN/SDS-PAGE), the first dimension BN-PAGE bands were excised and incubated for 15 min in denaturing and reducing buffer containing 1% SDS and 1% β-mercaptoethanol pH 6.4, and then incubated in a second buffer containing 1% SDS pH 6.4 for 15 min. Each lane was placed at the top of Bis-Tris Invitrogen™ Novex™ NuPAGE™ 4–12% acrylamide gradient gels and a gel solution (4% of acrylamide) was poured to seal the lane. PageRuler™ Plus (10 to 250 kDa) were loaded as a MW ladder. The migration was performed at 100 V for 1h30 in Novex™ MES running buffer according to the manufacturer recommendations.

Quantitative Western-blot analyses

For quantitative Western-blot analyses, 50 or 100 µg of protein extracts were solubilized in standard RIPA buffer containing 150 mM NaCl, 25 mM Tris-base pH 8.0, 1% (w/v) NP40, 1% (w/v) SDS, 0.25% (w/v) deoxycholate and 1 mM EGTA for 30 min at 4°C. The loading buffer containing 0.3 M Tris pH 6.8, 50% (w/v) glycerol, 30% (v/v) thioglycerol, 10% (w/v) SDS, 0.05% (w/v) bromophenol blue was added to the samples before incubating them at 75°C for 5 min. To obtain a good separation of small proteins we performed a denaturing Schägger gel using 15% of acrylamide gels as previously described (Schägger and von Jagow, 1987). A molecular weight marker, PageRuler™ Plus (10 to 250 kDa), was loaded on the gel. The denaturing electrophoresis was performed at 100 V for 2h. Proteins were then transferred onto nitrocellulose Amersham Protran Premium membrane (Amersham) (0.2 µm) with transfer buffer containing 25 mM Tris, 192 mM glycine, 0.1% (w/v) SDS at 100 V during 1h at 4°C. Membranes were stained with ponceau red solution containing 2 mg/ml ponceau red with 31% (v/v) acetic acid. After, membranes were incubated with blocking buffer containing 5% (w/v) skimmed milk diluted in PBS-tween buffer containing 10 mM NaH_2PO_4 pH 7.2, 0,14 M NaCl, 0,1% (w/v) Tween-20. For immunodetection, membranes were incubated with primary antibody diluted in PBS-tween and detected by a peroxidase-conjugated secondary antibody Clarity ECL reagent (Bio-Rad). The chemiluminescence signals were recorded using an ImageQuant (Amersham) and then quantified using ImageJ software.

If1 and Stf1 proteins were produced and purified to determine the relative abundance of both inhibitors in cells.

If1 was expressed and purified as mentioned in (Corvest et al., 2007), except that the His-tag was not removed. The *STF1* gene was amplified by PCR using the 5' - CGCGCGCCATGGCTGTTCTCATCATCATCATCACGACGGTCCTCGTGTGTGTGTGCCGG - 3' forward primer to introduce a N-terminal His-tag and the 5' CGCGCGCCATGGCTGTTCTCATCATCATCATCACGACGGTCCTCTCGTGTGTGTGTGTGCCGG - 3' reverse primer. The PCR product, digested by *Nco*1 and *Bam*H1, was inserted into the pIVEX2.3 vector and digested with the same restriction enzymes. The protein was produced in cell-free expression system (Larrieu et al., 2017). After 18 h of production at 28°C, the reaction mix was centrifuged (10 min, 12,000xg, 4°C) and the supernatant containing Stf1 was diluted 10-fold and loaded onto a Nickel NTA column. The column was washed with 25 column volumes of washing buffer 1 containing 150 mM NaCl,10 mM imidazole, 20 mM Tris-HCl pH 8.0, containing EDTA-free protease inhibitors (Pierce) and then with 20 column volumes of washing buffer 2 containing 150 mM NaCl, 20 mM imidazole, 20 mM Tris-HCl pH 8.0. The elution was performed with 4 column

volumes of elution buffer containing 150 mM NaCl, 250 mM Imidazole**,** 20 mM Tris-HCl pH 8.0 and EDTA-free protease inhibitors.

Antibodies

Primary antibodies: Pgk1 mouse monoclonal antibody 22C5D8 (CiteAb 459250), MTCO2 (Cox2) mouse monoclonal antibody (Thermo Fisher 12C4F12). Rabbit polyclonal antibodies raised against purified subunits β, ɣ, and subunit 4 were obtained in the laboratory. Rabbit polyclonal antibodies raised against the INDPRNPRFAKGGK peptide of subunit i were purchased from Neosystem. Anti-If1 antibodies were kindly provided by K. Tagawa (Osaka, Japan). The Stf1 protein produced *in vitro* was used by Covalab society to raise polyclonal rabbit antibodies.

The secondary antibodies used were: Peroxidase AffiniPure^{TM} Goat anti-rabbit IgG (Jackson ImmunoResearch AB_2313567); Peroxidase AffiniPure^{TM} Goat anti-mouse IgG (Jackson ImmunoResearch AB_2338504)

Metabolites quantifications

Cells were cultured for 12 h before adding 1 µM CCCP at 1 OD_{550nm}. After 1 h of treatment, size and number of cells were defined with a multisizer instrument. 20 ml of culture were filtered (Sartolon polyamid 0.45 µm) and the filter was rapidly rinsed twice with ice-cold water to stop reactions. Metabolites were extracted using an ethanol/20 mM HEPES pH 7.2 (2/8 v/v) solution as described (Ceschin et al., 2014). Metabolites were separated, detected and quantified on a High Performance Ion Chromatography (HPIC) station as described (Pinson et al., 2023). The intracellular concentration of nucleotides was determined using standard curves obtained with pure compounds. Adenylate energy charge was defined as AEC = [ATP] + ½ [ADP] / [ATP] + [ADP] + [AMP] (Atkinson and Walton, 1967).

Mitochondrial DNA quantification

For DNA extraction, cells were washed and broken by shaking during 1 min with an equal volume of glass beads (0.4 mm) in the following buffer: 10 mM Tris pH 8.0, 1 mM EDTA, 100 mM NaCl, 2% (v/v) Triton X-100, 1% (v/v) SDS and 50% (v/v) chloroform/phenol (1:1). Equal volumes of 10 mM Tris pH 8.0 and 1 mM EDTA buffer were added and vortexed during 5 min. The supernatant was mixed with an equal volume of chloroform during 1 min and centrifuged at 12,000g. The supernatant was mixed with a double volume of glacial ethanol and centrifuged at 12,000g. The pellet was dried at room temperature before being resuspended in nuclease-free water.

Quantitative PCR for mtDNA content were performed with qPCRBIO SyGreen Blue Mix Lo-ROX (Eurobio®). Based on the manufacturer's instructions, 0.1 ng of DNA was used to quantify mtDNA and nuclear DNA with two different sets of primers. The first mtDNA primer set (fw: TTGAAGCTGTACAACCTACC, rv: CCTGCGATTAAGGCATGATG) targeted a region of *COX3* gene, the second primer set (fw: AACAATTGGTTTATTAGGAGCAGGTATTGG, rv: TATACACCGAATAATAATAAGAATGAAACC) targeted a region of *ATP9* gene. The first nDNA primer set (fw: CACCCTGTTCTTTTGACTGA, rv: CATAGAAGGCTGGAACGTTG) targeted a region of *ACT1* gene, and the other primer set (fw: TGCTTTGTCAAATGGATCATATGG, rv: CCTGGAACCAAGTGAACAGTAC) targeted a region of *GAL1* gene.

Statistical analyses

Data are presented as mean ± SEM. Sample numbers (different culture) and experimental repeats are indicated in legends. Data were analyzed with the GraphPad Prism software using unpaired Student's t-test, one-way ANOVA or two-way ANOVA. A 0.05 p-value was considered statistically significant.

AUTHOR CONTRIBUTIONS

Dr Orane Lerouley performed and analyzed experiments. Dr. Benoit Pinson determined the quantification of metabolites. Isabelle Larrieu managed the production of the anti Stf1 antibody. Dr. Marie-France Giraud did the production and purification of IF1 and Stf1 for quantitative Western blot. Tom Ducrocq assisted Dr Orane Lerouley in generating and validating yeast mutant strains. Dr Arnaud Mourier and Dr Marie-France Giraud co-supervised the project, interpreted results and provided funding. AM administered, provided funding for the project and wrote the manuscript and all authors reviewed and edited the manuscript.

ACKNOWLEDGMENTS

We thank Deborah Tribouillard-Tanvier's team, Muriel Priault's team, Anne Devin's team and Derek McCusker's team for sharing advice, instruments, consumables and antibodies. Sabine Vaur and all members of the IBGC support team. We thank Dr Mairead Aubert for English proofreading of the manuscript. We thank also Claudine David for sharing precious advice and expertise and for her important support. The authors thank the staff of the SAM

platform from TBMCore unit (University of Bordeaux - CNRS UAR 3427 - INSERM US05) for quantification of nucleotides. The HPIC chromatography station used for nucleotide determination was purchased with the financial support of both SIRIC BRIO (COMUCAN) and the Region Nouvelle-Aquitaine (MetabOptic 2022-24564910, AAPPF2021-2020-12000110). This work was supported by grants from ANR (DynaMitoPatho ANR-22-CE14-0040) and University of Bordeaux.

References

Ackerman SH, Tzagoloff A. 1990. Identification of two nuclear genes (ATP11, ATP12) required for assembly of the yeast F1-ATPase. *Proc Natl Acad Sci U S A* **87**:4986–4990.

Anselmi C, Davies KM, Faraldo-Gómez JD. 2018. Mitochondrial ATP synthase dimers spontaneously associate due to a long-range membrane-induced force. *J Gen Physiol* **150**:763–770. doi:10.1085/jgp.201812033

Aßkamp MR, Klein M, Nevoigt E. 2019. Saccharomyces cerevisiae exhibiting a modified route for uptake and catabolism of glycerol forms significant amounts of ethanol from this carbon source considered as 'non-fermentable.' *Biotechnology for Biofuels* **12**:257. doi:10.1186/s13068-019-1597-2

Atkinson DE, Walton GM. 1967. Adenosine triphosphate conservation in metabolic regulation. Rat liver citrate cleavage enzyme. *J Biol Chem* **242**:3239–3241.

Blum TB, Hahn A, Meier T, Davies KM, Kühlbrandt W. 2019. Dimers of mitochondrial ATP synthase induce membrane curvature and self-assemble into rows. *Proceedings of the National Academy of Sciences* **116**:4250–4255. doi:10.1073/pnas.1816556116

Boreikaite V, Wicky BIM, Watt IN, Clarke J, Walker JE. 2019. Extrinsic conditions influence the self-association and structure of IF1, the regulatory protein of mitochondrial ATP synthase. *Proc Natl Acad Sci U S A* **116**:10354–10359. doi:10.1073/pnas.1903535116

Boyer PD, Cross RL, Momsen W. 1973. A New Concept for Energy Coupling in Oxidative Phosphorylation Based on a Molecular Explanation of the Oxygen Exchange Reactions. *Proc Natl Acad Sci U S A* **70**:2837–2839.

Buchanan BW, Lloyd ME, Engle SM, Rubenstein EM. 2016. Cycloheximide Chase Analysis of Protein Degradation in Saccharomyces cerevisiae. *J Vis Exp* 53975. doi:10.3791/53975

Buchet K, Godinot C. 1998. Functional F1-ATPase Essential in Maintaining Growth and Membrane Potential of Human Mitochondrial DNA-depleted ρ° Cells*. *Journal of Biological Chemistry* **273**:22983–22989. doi:10.1074/jbc.273.36.22983

Cabezón E, Arechaga I, Jonathan P, Butler G, Walker JE. 2000. Dimerization of bovine F1-ATPase by binding the inhibitor protein, IF1. *J Biol Chem* **275**:28353–28355. doi:10.1074/jbc.C000427200

Cabezon E, Butler PJG, Runswick MJ, Carbajo RJ, Walker JE. 2002. Homologous and heterologous inhibitory effects of ATPase inhibitor proteins on F-ATPases. *J Biol Chem* **277**:41334–41341. doi:10.1074/jbc.M207169200

Cabezon E, Butler PJG, Runswick MJ, Walker JE. 2000. Modulation of the Oligomerization State of the Bovine F1-ATPase Inhibitor Protein, IF1, by pH*. *Journal of Biological Chemistry* **275**:25460–25464. doi:10.1074/jbc.M003859200

Cabezón E, Runswick MJ, Leslie AG, Walker JE. 2001. The structure of bovine IF(1), the regulatory subunit of mitochondrial F-ATPase. *EMBO J* **20**:6990–6996. doi:10.1093/emboj/20.24.6990

Carroll J, Watt IN, Wright CJ, Ding S, Fearnley IM, Walker JE. 2024. The inhibitor protein IF1 from mammalian mitochondria inhibits ATP hydrolysis but not ATP synthesis by the ATP synthase complex. *Journal of Biological Chemistry* **300**. doi:10.1016/j.jbc.2024.105690

Carrozzo R, Wittig I, Santorelli FM, Bertini E, Hofmann S, Brandt U, Schägger H. 2006. Subcomplexes of human ATP synthase mark mitochondrial biosynthesis disorders. *Annals of Neurology* **59**:265–275. doi:10.1002/ana.20729

Ceschin J, Saint-Marc C, Laporte J, Labriet A, Philippe C, Moenner M, Daignan-Fornier B, Pinson

B. 2014. Identification of yeast and human 5-aminoimidazole-4-carboxamide-1-β-d-ribofuranoside (AICAr) transporters. *J Biol Chem* **289**:16844–16854. doi:10.1074/jbc.M114.551192

Chen XJ, Clark-Walker GD. 1999. α and β subunits of F1-ATPase are required for survival of petite mutants in Saccharomyces cerevisiae. *Mol Gen Genet* **262**:898–908. doi:10.1007/s004380051156

Cintrón NM, Pedersen PL. 1979. A protein inhibitor of the mitochondrial adenosine triphosphatase complex of rat liver. Purification and characterization. *J Biol Chem* **254**:3439–3443.

Clark-Walker GD. 2007. The F1-ATPase inhibitor Inh1 (IF1) affects suppression of mtDNA loss-lethality in Kluyveromyces lactis. *FEMS Yeast Research* **7**:665–674. doi:10.1111/j.1567-1364.2006.00201.x

Corvest V, Sigalat C, Haraux F. 2007. Insight into the Bind−Lock Mechanism of the Yeast Mitochondrial ATP Synthase Inhibitory Peptide. *Biochemistry* **46**:8680–8688. doi:10.1021/bi700522v

Courbon GM, Rubinstein JL. 2022. CryoEM Reveals the Complexity and Diversity of ATP Synthases. *Front Microbiol* **13**. doi:10.3389/fmicb.2022.864006

Davies KM, Anselmi C, Wittig I, Faraldo-Gómez JD, Kühlbrandt W. 2012. Structure of the yeast F1Fo-ATP synthase dimer and its role in shaping the mitochondrial cristae. *Proc Natl Acad Sci U S A* **109**:13602–13607. doi:10.1073/pnas.1204593109

Devin A, Dejean L, Beauvoit B, Chevtzoff C, Avéret N, Bunoust O, Rigoulet M. 2006. Growth yield homeostasis in respiring yeast is due to a strict mitochondrial content adjustment. *J Biol Chem* **281**:26779–26784. doi:10.1074/jbc.M604800200

Dienhart M, Pfeiffer K, Schägger H, Stuart RA. 2002. Formation of the Yeast F1F0-ATP Synthase Dimeric Complex Does Not Require the ATPase Inhibitor Protein, Inh1*. *Journal of Biological Chemistry* **277**:39289–39295. doi:10.1074/jbc.M205720200

Domínguez-Zorita S, Romero-Carramiñana I, Santacatterina F, Esparza-Moltó PB, Simó C, Del-Arco A, Núñez de Arenas C, Saiz J, Barbas C, Cuezva JM. 2023. IF1 ablation prevents ATP synthase oligomerization, enhances mitochondrial ATP turnover and promotes an adenosine-mediated pro-inflammatory phenotype. *Cell Death Dis* **14**:413. doi:10.1038/s41419-023-05957-z

Dupont C-H, Mazat JP, Guerin B. 1985. The role of adenine nucleotide translocation in the energization of the inner membrane of mitochondria isolated from ϱ+ and ϱo strains of saccharomyces cerevisiae. *Biochemical and Biophysical Research Communications* **132**:1116–1123. doi:10.1016/0006-291X(85)91922-9

Fernández-Cárdenas LP, Villanueva-Chimal E, Salinas LS, José-Nuñez C, Tuena de Gómez Puyou M, Navarro RE. 2017. Caenorhabditis elegans ATPase inhibitor factor 1 (IF1) MAI-2 preserves the mitochondrial membrane potential (Δψm) and is important to induce germ cell apoptosis. *PLoS One* **12**:e0181984. doi:10.1371/journal.pone.0181984

Galber C, Carissimi S, Baracca A, Giorgio V. 2021. The ATP Synthase Deficiency in Human Diseases. *Life (Basel)* **11**:325. doi:10.3390/life11040325

Galkina KV, Zubareva VM, Kashko ND, Lapashina AS, Markova OV, Feniouk BA, Knorre DA. 2022. Heterogeneity of Starved Yeast Cells in IF1 Levels Suggests the Role of This Protein in vivo. *Front Microbiol* **13**:816622. doi:10.3389/fmicb.2022.816622

García-Bermúdez J, Sánchez-Aragó M, Soldevilla B, Del Arco A, Nuevo-Tapioles C, Cuezva JM. 2015. PKA Phosphorylates the ATPase Inhibitory Factor 1 and Inactivates Its Capacity to Bind and Inhibit the Mitochondrial H(+)-ATP Synthase. *Cell Rep* **12**:2143–2155. doi:10.1016/j.celrep.2015.08.052

Gatto C, Grandi M, Solaini G, Baracca A, Giorgio V. 2022. The F1Fo-ATPase inhibitor protein IF1 in pathophysiology. *Front Physiol* **13**:917203. doi:10.3389/fphys.2022.917203

Giraud M-F, Velours J. 1997. The Absence of the Mitochondrial ATP Synthase □ Subunit Promotes a Slow Growth Phenotype of Rho− Yeast Cells by a Lack of Assembly of the Catalytic Sector F1. *European Journal of Biochemistry* **245**:813–818. doi:10.1111/j.1432-1033.1997.00813.x

Gu J, Zhang L, Zong S, Guo R, Liu T, Yi J, Wang P, Zhuo W, Yang M. 2019. Cryo-EM structure of the mammalian ATP synthase tetramer bound with inhibitory protein IF1. *Science* **364**:1068–1075. doi:10.1126/science.aaw4852

Guérin B, Labbe P, Somlo M. 1979. [19] Preparation of yeast mitochondria (*Saccharomyces cerevisiae*) with good P/O and respiratory control ratiosMethods in Enzymology, Biomembranes

Part F: Bioenergetics: Oxidative Phosphorylation. Academic Press. pp. 149–159. doi:10.1016/0076-6879(79)55021-6

Hahn A, Parey K, Bublitz M, Mills DJ, Zickermann V, Vonck J, Kühlbrandt W, Meier T. 2016. Structure of a Complete ATP Synthase Dimer Reveals the Molecular Basis of Inner Mitochondrial Membrane Morphology. *Mol Cell* **63**:445–456. doi:10.1016/j.molcel.2016.05.037

Hahn A, Vonck J, Mills DJ, Meier T, Kühlbrandt W. 2018. Structure, mechanism, and regulation of the chloroplast ATP synthase. *Science* **360**:eaat4318. doi:10.1126/science.aat4318

Hashimoto T, Negawa Y, Tagawa K. 1981. Binding of intrinsic ATPase inhibitor to mitochondrial ATPase--stoichiometry of binding of nucleotides, inhibitor, and enzyme. *J Biochem* **90**:1151–1157. doi:10.1093/oxfordjournals.jbchem.a133567

Hashimoto T, Yoshida Y, Tagawa K. 1990. Simultaneous bindings of ATPase inhibitor and 9K protein to F1F0-ATPase in the presence of 15K protein in yeast mitochondria. *J Biochem* **108**:17–20. doi:10.1093/oxfordjournals.jbchem.a123154

Hashimoto T, Yoshida Y, Tagawa K. 1987. Binding properties of 9K protein to F1-ATPase: a counterpart ligand to the ATPase inhibitor. *J Biochem* **102**:685–692. doi:10.1093/oxfordjournals.jbchem.a122106

Hashimoto T, Yoshida Y, Tagawa K. 1984. Purification and properties of factors in yeast mitochondria stabilizing the F1F0-ATPase-inhibitor complex. *J Biochem* **95**:131–136. doi:10.1093/oxfordjournals.jbchem.a134576

He J, Ford HC, Carroll J, Douglas C, Gonzales E, Ding S, Fearnley IM, Walker JE. 2018. Assembly of the membrane domain of ATP synthase in human mitochondria. *Proceedings of the National Academy of Sciences* **115**:2988–2993. doi:10.1073/pnas.1722086115

Hong S, Pedersen PL. 2002. ATP synthase of yeast: structural insight into the different inhibitory potencies of two regulatory peptides and identification of a new potential regulator. *Archives of Biochemistry and Biophysics* **405**:38–43. doi:10.1016/S0003-9861(02)00303-X

Ichikawa N, Ogura C. 2003. Overexpression, purification, and characterization of human and bovine mitochondrial ATPase inhibitors: comparison of the properties of mammalian and yeast ATPase inhibitors. *J Bioenerg Biomembr* **35**:399–407. doi:10.1023/a:1027383629565

Ichikawa N, Yoshida Y, Hashimoto T, Ogasawara N, Yoshikawa H, Imamoto F, Tagawa K. 1990. Activation of ATP hydrolysis by an uncoupler in mutant mitochondria lacking an intrinsic ATPase inhibitor in yeast. *Journal of Biological Chemistry* **265**:6274–6278. doi:10.1016/S0021-9258(19)39321-4

Jänsch L, Kruft V, Schmitz UK, Braun HP. 1996. New insights into the composition, molecular mass and stoichiometry of the protein complexes of plant mitochondria. *Plant J* **9**:357–368. doi:10.1046/j.1365-313x.1996.09030357.x

Kominsky DJ, Brownson MP, Updike DL, Thorsness PE. 2002. Genetic and Biochemical Basis for Viability of Yeast Lacking Mitochondrial Genomes. *Genetics* **162**:1595–1604. doi:10.1093/genetics/162.4.1595

Kovácová V, Irmlerová J, Kovác L. 1968. Oxidative phosphorylatiion in yeast. IV. Combination of a nuclear mutation affecting oxidative phosphorylation with cytoplasmic mutation to respiratory deficiency. *Biochim Biophys Acta* **162**:157–163. doi:10.1016/0005-2728(68)90097-2

Kühlbrandt W. 2019. Structure and Mechanisms of F-Type ATP Synthases. *Annu Rev Biochem* **88**:515–549. doi:10.1146/annurev-biochem-013118-110903

Larrieu I, Tolchard J, Sanchez C, Kone EY, Barras A, Stines-Chaumeil C, Odaert B, Giraud M-F. 2017. Cell-Free Expression for the Study of Hydrophobic Proteins: The Example of Yeast ATP-Synthase Subunits In: Lacapere J-J, editor. Membrane Protein Structure and Function Characterization: Methods and Protocols. New York, NY: Springer. pp. 57–90. doi:10.1007/978-1-4939-7151-0_4

Lau WCY, Baker LA, Rubinstein JL. 2008. Cryo-EM structure of the yeast ATP synthase. *J Mol Biol* **382**:1256–1264. doi:10.1016/j.jmb.2008.08.014

Le Breton N, Adrianaivomananjaona T, Gerbaud G, Etienne E, Bisetto E, Dautant A, Guigliarelli B, Haraux F, Martinho M, Belle V. 2016. Dimerization interface and dynamic properties of yeast IF1 revealed by Site-Directed Spin Labeling EPR spectroscopy. *Biochim Biophys Acta* **1857**:89–97. doi:10.1016/j.bbabio.2015.10.010

Li L, Carrie C, Nelson C, Whelan J, Millar AH. 2012. Accumulation of newly synthesized F1 in vivo in arabidopsis mitochondria provides evidence for modular assembly of the plant F1Fo ATP synthase. *J Biol Chem* **287**:25749–25757. doi:10.1074/jbc.M112.373506

Liu Siqi, Liu Shanshan, He B, Li Lanlan, Li Lin, Wang J, Cai T, Chen S, Jiang H. 2021. OXPHOS deficiency activates global adaptation pathways to maintain mitochondrial membrane potential. *EMBO reports* **22**:e51606. doi:10.15252/embr.202051606

Lucero R-A, Mercedes E-P, Thorsten L, Giovanni G-C, Michael F, Guadalupe Z, Pablo PJ, Federico M, Oscar F-H. 2021. Deletion of the natural inhibitory protein Inh1 in *Ustilago maydis* has no effect on the dimeric state of the F1FO-ATP synthase but increases the ATPase activity and reduces the stability. *Biochimica et Biophysica Acta (BBA) - Bioenergetics* **1862**:148429. doi:10.1016/j.bbabio.2021.148429

Matsubara H, Hase T, Hashimoto T, Tagawa K. 1981. Amino acid sequence of an intrinsic inhibitor of mitochondrial ATPase from yeast. *J Biochem* **90**:1159–1165. doi:10.1093/oxfordjournals.jbchem.a133568

Mitchell P. 1961. Coupling of phosphorylation to electron and hydrogen transfer by a chemi-osmotic type of mechanism. *Nature* **191**:144–148. doi:10.1038/191144a0

Molinié T, Cougouilles E, David C, Cahoreau E, Portais J-C, Mourier A. 2022. MDH2 produced OAA is a metabolic switch rewiring the fuelling of respiratory chain and TCA cycle. *Biochim Biophys Acta Bioenerg* **1863**:148532. doi:10.1016/j.bbabio.2022.148532

Mourier A, Devin A, Rigoulet M. 2010. Active proton leak in mitochondria: a new way to regulate substrate oxidation. *Biochim Biophys Acta* **1797**:255–261. doi:10.1016/j.bbabio.2009.10.011

Mourier A, Ruzzenente B, Brandt T, Kühlbrandt W, Larsson N-G. 2014. Loss of LRPPRC causes ATP synthase deficiency. *Hum Mol Genet* **23**:2580–2592. doi:10.1093/hmg/ddt652

Mühleip A, Kock Flygaard R, Ovciarikova J, Lacombe A, Fernandes P, Sheiner L, Amunts A. 2021. ATP synthase hexamer assemblies shape cristae of Toxoplasma mitochondria. *Nat Commun* **12**:120. doi:10.1038/s41467-020-20381-z

Nakamura J, Fujikawa M, Yoshida M. 2013. IF1, a natural inhibitor of mitochondrial ATP synthase, is not essential for the normal growth and breeding of mice. *Biosci Rep* **33**:e00067. doi:10.1042/BSR20130078

Nijtmans LGJ, Klement P, Houštěk J, van den Bogert C. 1995. Assembly of mitochondrial ATP synthase in cultured human cells: implications for mitochondrial diseases. *Biochimica et Biophysica Acta (BBA) - Molecular Basis of Disease* **1272**:190–198. doi:10.1016/0925-4439(95)00087-9

Norling B, Tourikas C, Hamasur B, Glaser E. 1990. Evidence for an endogenous ATPase inhibitor protein in plant mitochondria. Purification and characterization. *Eur J Biochem* **188**:247–252. doi:10.1111/j.1432-1033.1990.tb15396.x

Paul M-F, Velours J, ARSELIN de CHATEAUBODEAU G, Aigle M, Guerin B. 1989. The role of subunit 4, a nuclear-encoded protein of the F0 sector of yeast mitochondrial ATP synthase, in the assembly of the whole complex. *European Journal of Biochemistry* **185**:163–171. doi:10.1111/j.1432-1033.1989.tb15098.x

Pietrobon D, Zoratti M, Azzone GF. 1983. Molecular slipping in redox and ATPase H+ pumps. *Biochimica et Biophysica Acta (BBA) - Bioenergetics* **723**:317–321. doi:10.1016/0005-2728(83)90131-7

Pinke G, Zhou L, Sazanov LA. 2020. Cryo-EM structure of the entire mammalian F-type ATP synthase. *Nat Struct Mol Biol* **27**:1077–1085. doi:10.1038/s41594-020-0503-8

Pinson B, Moenner M, Saint-Marc C, Granger-Farbos A, Daignan-Fornier B. 2023. On-demand utilization of phosphoribosyl pyrophosphate by downstream anabolic pathways. *J Biol Chem* **299**:105011. doi:10.1016/j.jbc.2023.105011

Pullman ME, Monroy GC. 1963. A Naturally Occurring Inhibitor of Mitochondrial Adenosine Triphosphatase. *Journal of Biological Chemistry* **238**:3762–3769. doi:10.1016/S0021-9258(19)75338-1

Robinson GC, Bason JV, Montgomery MG, Fearnley IM, Mueller DM, Leslie AGW, Walker JE. 2013. The structure of F1-ATPase from Saccharomyces cerevisiae inhibited by its regulatory protein IF1. *Open Biology* **3**:120164. doi:10.1098/rsob.120164

Romero-Carramiñana I, Esparza-Moltó PB, Domínguez-Zorita S, Nuevo-Tapioles C, Cuezva JM.

2023. IF1 promotes oligomeric assemblies of sluggish ATP synthase and outlines the heterogeneity of the mitochondrial membrane potential. *Commun Biol* **6**:1–16. doi:10.1038/s42003-023-05214-1

Rouslin W, Broge CW. 1996. IF1 function in situ in uncoupler-challenged ischemic rabbit, rat, and pigeon hearts. *J Biol Chem* **271**:23638–23641. doi:10.1074/jbc.271.39.23638

Sánchez-Aragó M, Formentini L, Martínez-Reyes I, García-Bermudez J, Santacatterina F, Sánchez-Cenizo L, Willers IM, Aldea M, Nájera L, Juarránz A, López EC, Clofent J, Navarro C, Espinosa E, Cuezva JM. 2013. Expression, regulation and clinical relevance of the ATPase inhibitory factor 1 in human cancers. *Oncogenesis* **2**:e46. doi:10.1038/oncsis.2013.9

Sánchez-Cenizo L, Formentini L, Aldea M, Ortega AD, García-Huerta P, Sánchez-Aragó M, Cuezva JM. 2010. Up-regulation of the ATPase inhibitory factor 1 (IF1) of the mitochondrial H+-ATP synthase in human tumors mediates the metabolic shift of cancer cells to a Warburg phenotype. *J Biol Chem* **285**:25308–25313. doi:10.1074/jbc.M110.146480

Schägger H, von Jagow G. 1987. Tricine-sodium dodecyl sulfate-polyacrylamide gel electrophoresis for the separation of proteins in the range from 1 to 100 kDa. *Analytical Biochemistry* **166**:368–379. doi:10.1016/0003-2697(87)90587-2

Senior AE. 1988. ATP synthesis by oxidative phosphorylation. *Physiological Reviews* **68**:177–231. doi:10.1152/physrev.1988.68.1.177

Sgarbi G, Barbato S, Costanzini A, Solaini G, Baracca A. 2018. The role of the ATPase inhibitor factor 1 (IF1) in cancer cells adaptation to hypoxia and anoxia. *Biochimica et Biophysica Acta (BBA) - Bioenergetics* **1859**:99–109. doi:10.1016/j.bbabio.2017.10.007

Sinha SD, Wideman JG. 2023. The persistent homology of mitochondrial ATP synthases. *iScience* **26**:106700. doi:10.1016/j.isci.2023.106700

Sprague GF. 1977. Isolation and characterization of a Saccharomyces cerevisiae mutant deficient in pyruvate kinase activity. *J Bacteriol* **130**:232–241.

Stock D, Leslie AGW, Walker JE. 1999. Molecular Architecture of the Rotary Motor in ATP Synthase. *Science* **286**:1700–1705. doi:10.1126/science.286.5445.1700

Subík J, Kolarov J, Kovác L. 1972. Obligatory requirement of intramitochondrial ATP for normal functioning of the eucaryotic cell. *Biochem Biophys Res Commun* **49**:192–198. doi:10.1016/0006-291x(72)90028-9

Tzagoloff A. 1969. Assembly of the mitochondrial membrane system. II. Synthesis of the mitochondrial adenosine triphosphatase. F1. *J Biol Chem* **244**:5027–5033.

Tzagoloff A, Akai A, Needleman R. 1975. Assembly of the mitochondrial membrane system. Characterization of nuclear mutants of Saccharomyces cerevisiae with defects in mitochondrial ATPase and respiratory enzymes. *Journal of Biological Chemistry* **250**:8228–8235. doi:10.1016/S0021-9258(19)40840-5

Vaillier J, Arselin G, Graves P-V, Camougrand N, Velours J. 1999. Isolation of Supernumerary Yeast ATP Synthase Subunits e and i: CHARACTERIZATION OF SUBUNIT i AND DISRUPTION OF ITS STRUCTURAL GENE ATP18 *. *Journal of Biological Chemistry* **274**:543–548. doi:10.1074/jbc.274.1.543

Venard R, Brèthes D, Giraud M-F, Vaillier J, Velours J, Haraux F. 2003. Investigation of the Role and Mechanism of IF1 and STF1 Proteins, Twin Inhibitory Peptides Which Interact with the Yeast Mitochondrial ATP Synthase. *Biochemistry* **42**:7626–7636. doi:10.1021/bi034394t

Wagner K, Perschil I, Fichter CD, van der Laan M. 2010. Stepwise assembly of dimeric F(1)F(o)-ATP synthase in mitochondria involves the small F(o)-subunits k and i. *Mol Biol Cell* **21**:1494–1504. doi:10.1091/mbc.e09-12-1023

Watt IN, Montgomery MG, Runswick MJ, Leslie AGW, Walker JE. 2010. Bioenergetic cost of making an adenosine triphosphate molecule in animal mitochondria. *Proceedings of the National Academy of Sciences* **107**:16823–16827. doi:10.1073/pnas.1011099107

Weissert V, Rieger B, Morris S, Arroum T, Psathaki OE, Zobel T, Perkins G, Busch KB. 2021. Inhibition of the mitochondrial ATPase function by IF1 changes the spatiotemporal organization of ATP synthase. *Biochimica et Biophysica Acta (BBA) - Bioenergetics* **1862**:148322. doi:10.1016/j.bbabio.2020.148322

Wittig I, Carrozzo R, Santorelli FM, Schägger H. 2006. Supercomplexes and subcomplexes of mitochondrial oxidative phosphorylation. *Biochim Biophys Acta* **1757**:1066–1072.

doi:10.1016/j.bbabio.2006.05.006
Wittig I, Karas M, Schägger H. 2007. High Resolution Clear Native Electrophoresis for In-gel Functional Assays and Fluorescence Studies of Membrane Protein Complexes*. *Molecular & Cellular Proteomics* **6**:1215–1225. doi:10.1074/mcp.M700076-MCP200
Wittig I, Meyer B, Heide H, Steger M, Bleier L, Wumaier Z, Karas M, Schägger H. 2010. Assembly and oligomerization of human ATP synthase lacking mitochondrial subunits a and A6L. *Biochimica et Biophysica Acta (BBA) - Bioenergetics*, 16th European Bioenergetics Conference 2010 **1797**:1004–1011. doi:10.1016/j.bbabio.2010.02.021
Xiberras J, Klein M, Nevoigt E. 2019. Glycerol as a substrate for *Saccharomyces cerevisiae* based bioprocesses – Knowledge gaps regarding the central carbon catabolism of this 'non-fermentable' carbon source. *Biotechnology Advances*, Microbial Engineering Biotechnologies **37**:107378. doi:10.1016/j.biotechadv.2019.03.017
Yang J-H, Williams D, Kandiah E, Fromme P, Chiu P-L. 2020. Structural basis of redox modulation on chloroplast ATP synthase. *Commun Biol* **3**:1–12. doi:10.1038/s42003-020-01221-8

Figure 1

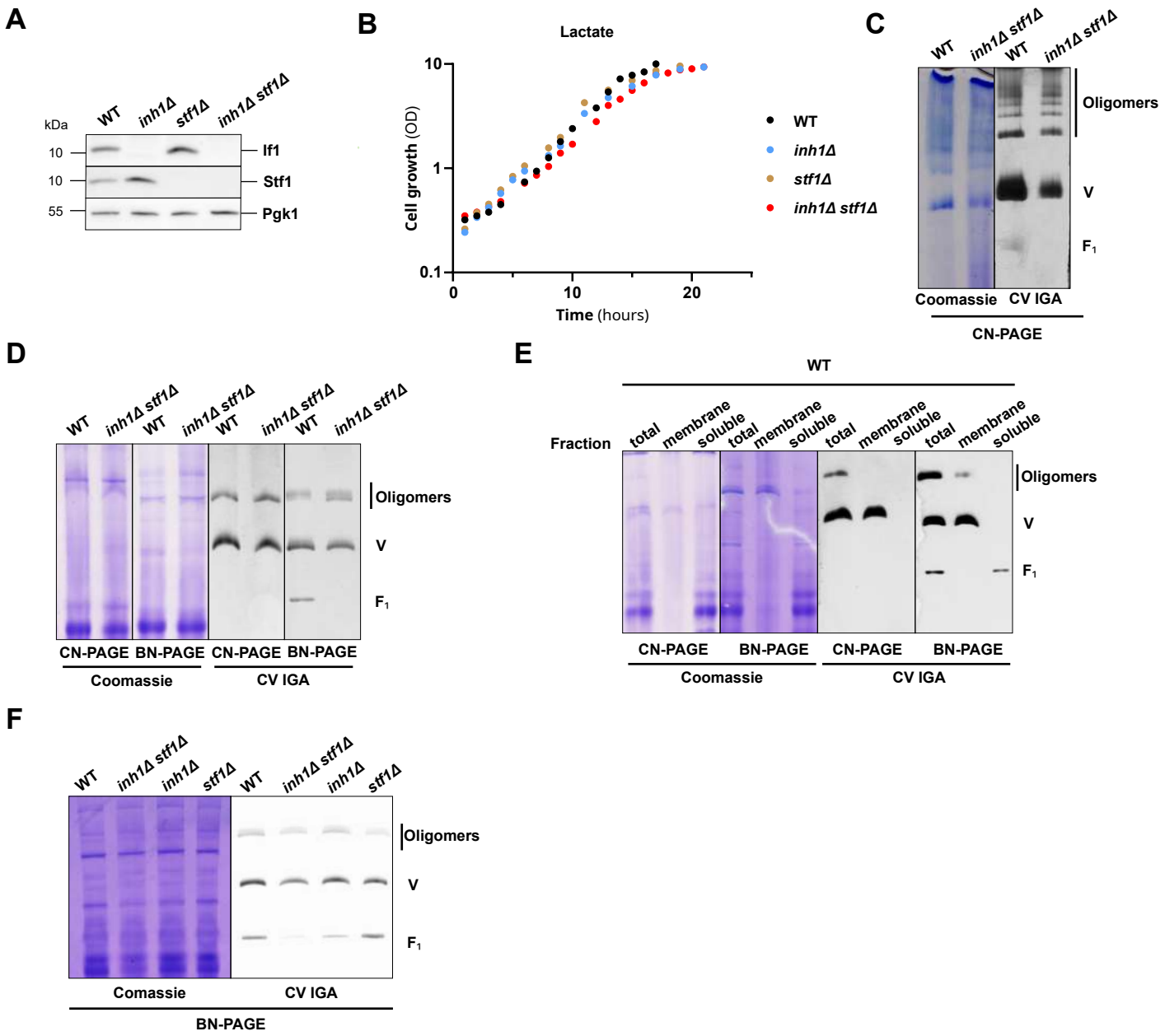
A
kDa
WT
inh1Δ
stf1Δ
inh1Δ stf1Δ
10
10
55
If1
Stf1
Pgk1
B
Lactate
Cell growth (OD)
10
1
0.1
0
10
20
Time (hours)
WT
inh1Δ
stf1Δ
inh1Δ stf1Δ
C
WT
inh1Δ stf1Δ
WT
inh1Δ stf1Δ
Oligomers
V
F1
Coomassie
CV IGA
CN-PAGE
D
WT
inh1Δ stf1Δ
WT
inh1Δ stf1Δ
WT
inh1Δ stf1Δ
WT
inh1Δ stf1Δ
Oligomers
V
F1
CN-PAGE
BN-PAGE
CN-PAGE
BN-PAGE
Coomassie
CV IGA
E
WT
Fraction
total
membrane
soluble
total
membrane
soluble
total
membrane
soluble
total
membrane
soluble
Oligomers
V
F1
CN-PAGE
BN-PAGE
CN-PAGE
BN-PAGE
Coomassie
CV IGA
F
WT
inh1Δ stf1Δ
inh1Δ
stf1Δ
WT
inh1Δ stf1Δ
inh1Δ
stf1Δ
Oligomers
V
F1
Comassie
CV IGA
BN-PAGE

Figure 2

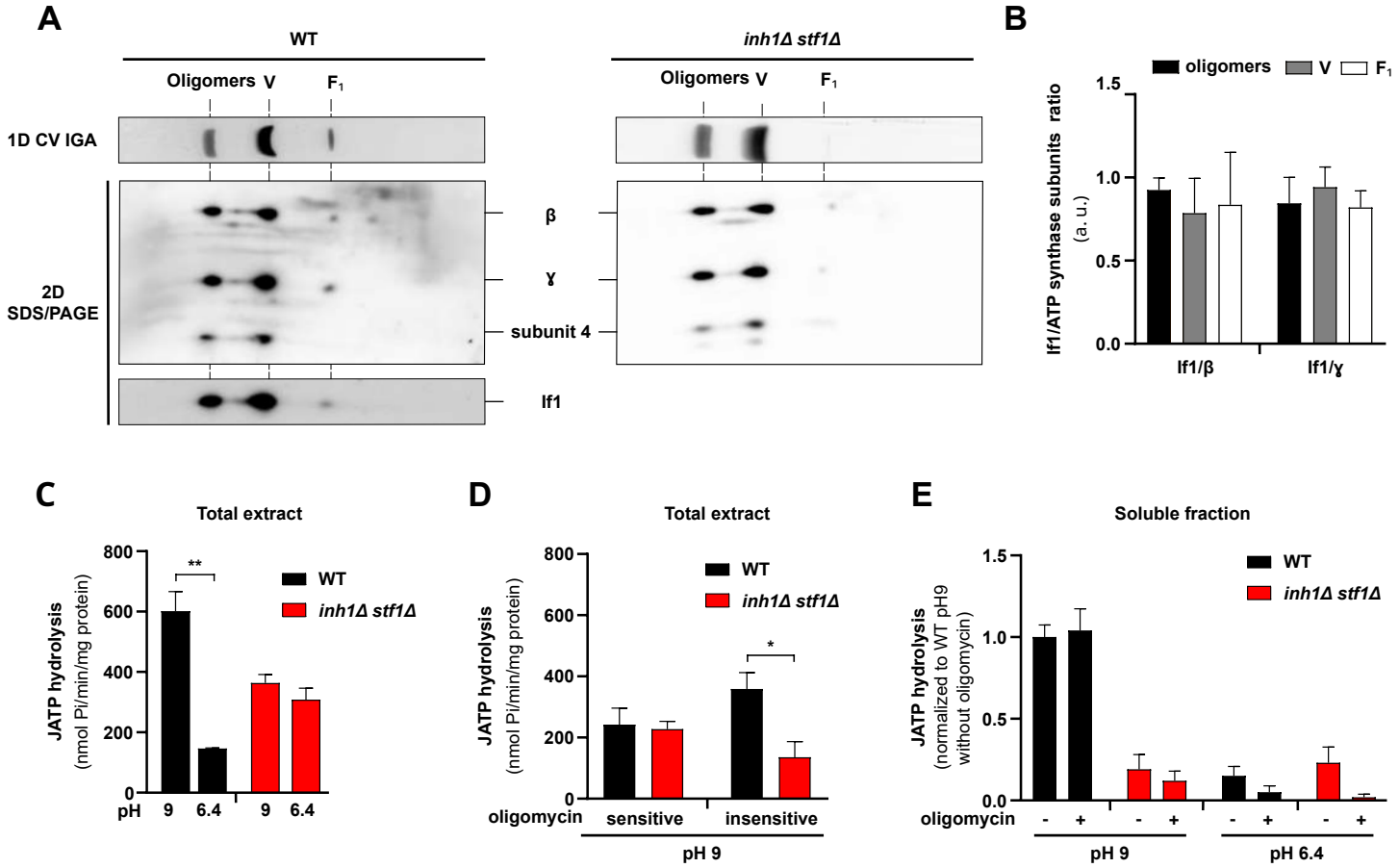
A
WT
inh1Δ stf1Δ
Oligomers V
F1
1D CV IGA
2D SDS/PAGE
β
γ
subunit 4
If1
B
oligomers
V
F1
If1/ATP synthase subunits ratio (a. u.)
1.5
1.0
0.5
0.0
If1/β
If1/γ
C
Total extract
JATP hydrolysis (nmol Pi/min/mg protein)
800
600
400
200
0
**
WT
inh1Δ stf1Δ
pH 9 6.4 9 6.4
D
Total extract
JATP hydrolysis (nmol Pi/min/mg protein)
*
oligomycin sensitive insensitive
pH 9
E
Soluble fraction
JATP hydrolysis (normalized to WT pH9 without oligomycin)
oligomycin - + - + - + - +
pH 9
pH 6.4

Figure 3

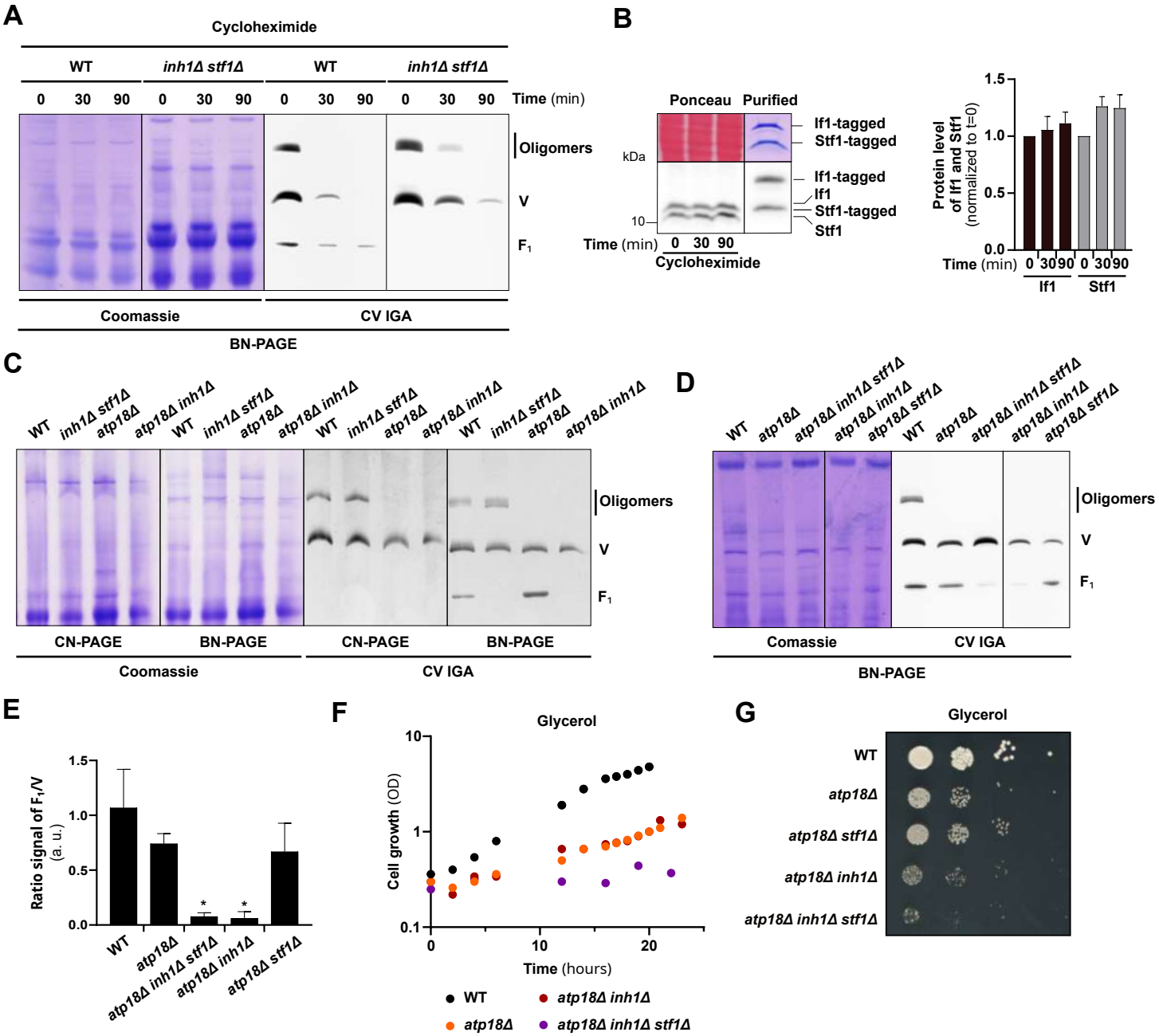
A
Cycloheximide
WT
inh1Δ stf1Δ
WT
inh1Δ stf1Δ
0 30 90 0 30 90 0 30 90 0 30 90
Time (min)
Oligomers
V
F1
Coomassie
CV IGA
BN-PAGE
B
Ponceau
Purified
kDa
10
If1-tagged
Stf1-tagged
If1-tagged
If1
Stf1-tagged
Stf1
Time (min) 0 30 90
Cycloheximide
Protein level of If1 and Stf1 (normalized to t=0)
1.5
1.0
0.5
0.0
Time (min) 0 30 90 0 30 90
If1
Stf1
C
WT
inh1Δ stf1Δ
atp18Δ
atp18Δ inh1Δ
Oligomers
V
F1
CN-PAGE
BN-PAGE
CN-PAGE
BN-PAGE
Coomassie
CV IGA
D
WT
atp18Δ
atp18Δ inh1Δ stf1Δ
atp18Δ inh1Δ
atp18Δ stf1Δ
Oligomers
V
F1
Comassie
CV IGA
BN-PAGE
E
Ratio signal of F1/V (a. u.)
1.5
1.0
0.5
0.0
*
*
WT
atp18Δ
atp18Δ inh1Δ stf1Δ
atp18Δ inh1Δ
atp18Δ stf1Δ
F
Glycerol
Cell growth (OD)
10
1
0.1
0
10
20
Time (hours)
WT
atp18Δ
atp18Δ inh1Δ
atp18Δ inh1Δ stf1Δ
G
Glycerol
WT
atp18Δ
atp18Δ stf1Δ
atp18Δ inh1Δ
atp18Δ inh1Δ stf1Δ

Figure 4

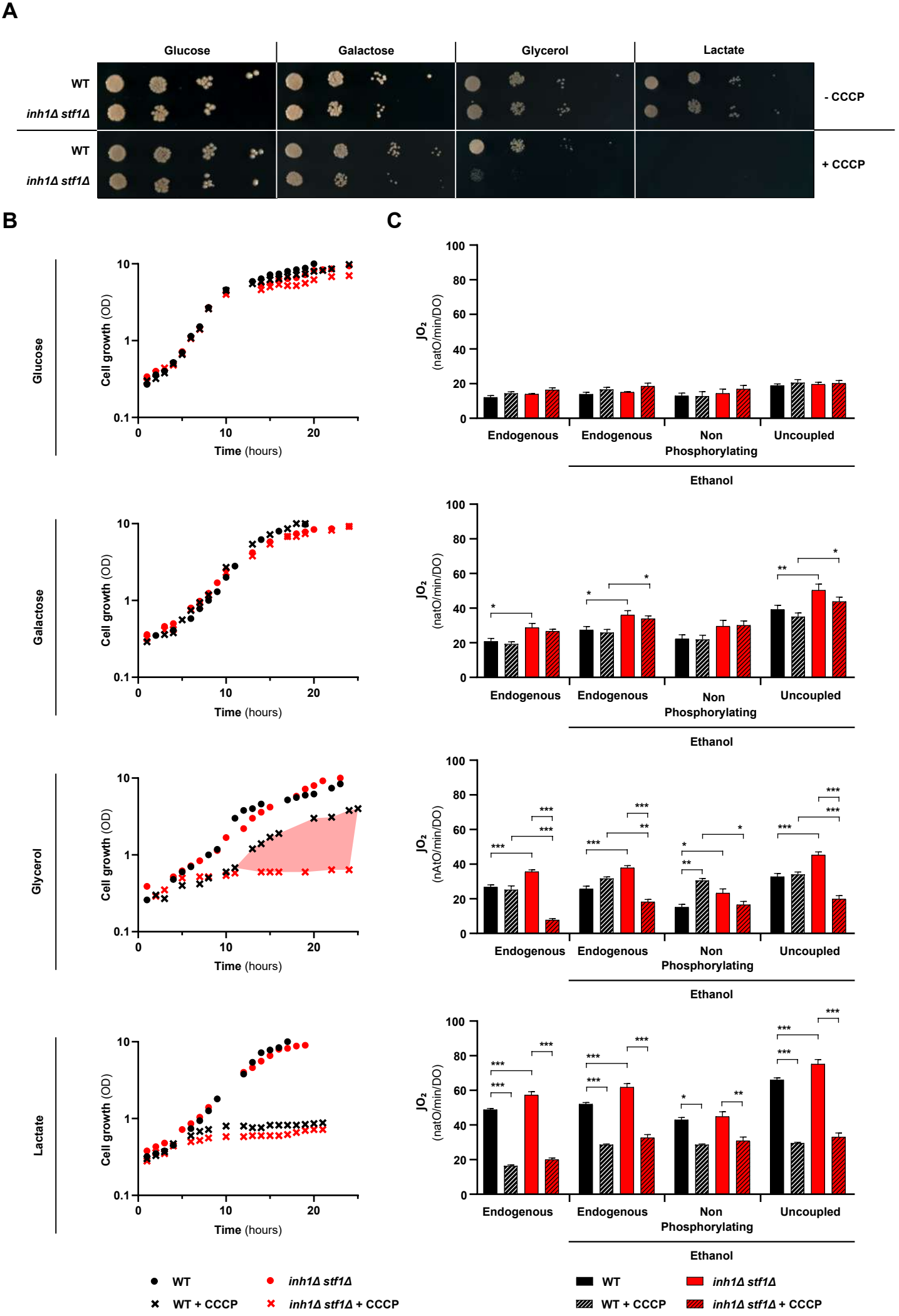
A
Glucose
Galactose
Glycerol
Lactate
WT
inh1Δ stf1Δ
- CCCP
+ CCCP
B
C
Glucose
Galactose
Glycerol
Lactate
Cell growth (OD)
Time (hours)
JO2 (natO/min/DO)
JO2 (nAtO/min/DO)
Endogenous
Endogenous
Non Phosphorylating
Uncoupled
Ethanol
WT
inh1Δ stf1Δ
WT + CCCP
inh1Δ stf1Δ + CCCP

Figure 5

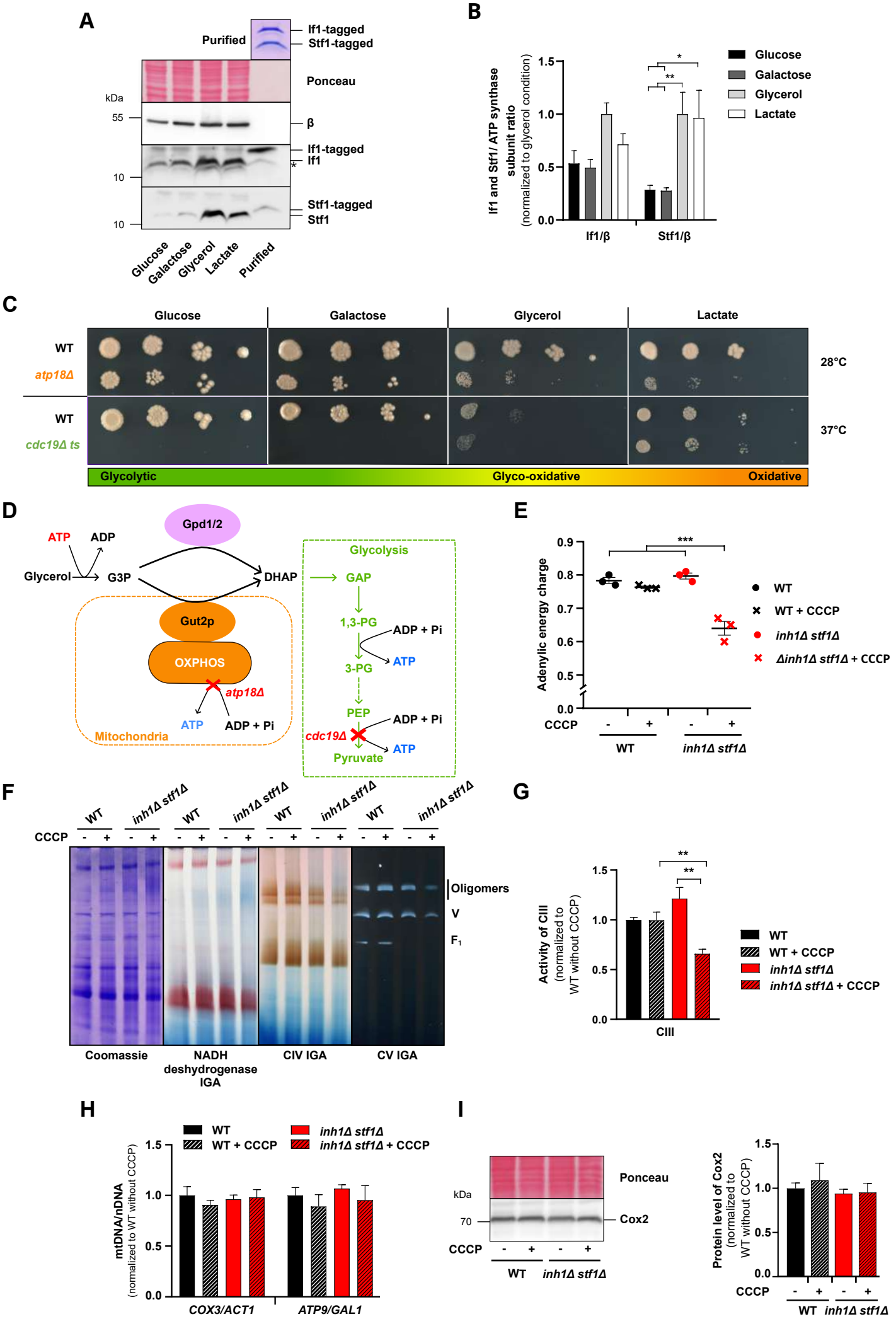
A
Purified
If1-tagged
Stf1-tagged
Ponceau
kDa
55
β
If1-tagged
If1
*
10
Stf1-tagged
Stf1
10
Glucose
Galactose
Glycerol
Lactate
Purified
B
If1 and Stf1/ ATP synthase subunit ratio (normalized to glycerol condition)
1.5
1.0
0.5
0.0
*
**
If1/β
Stf1/β
Glucose
Galactose
Glycerol
Lactate
C
Glucose
Galactose
Glycerol
Lactate
WT
atp18Δ
28°C
WT
cdc19Δ ts
37°C
Glycolytic
Glyco-oxidative
Oxidative
D
Gpd1/2
ATP
ADP
Glycerol
G3P
DHAP
Gut2p
OXPHOS
atp18Δ
ATP
ADP + Pi
Mitochondria
Glycolysis
GAP
1,3-PG
ADP + Pi
ATP
3-PG
PEP
ADP + Pi
cdc19Δ
ATP
Pyruvate
E
Adenylic energy charge
0.9
0.8
0.7
0.6
0.5
0.0
***
CCCP
-
+
-
+
WT
inh1Δ stf1Δ
WT
WT + CCCP
inh1Δ stf1Δ
Δinh1Δ stf1Δ + CCCP
F
WT
inh1Δ stf1Δ
CCCP
- +
Oligomers
V
F1
Coomassie
NADH deshydrogenase IGA
CIV IGA
CV IGA
G
Activity of CIII (normalized to WT without CCCP)
1.5
1.0
0.5
0.0
**
**
CIII
WT
WT + CCCP
inh1Δ stf1Δ
inh1Δ stf1Δ + CCCP
H
WT
WT + CCCP
inh1Δ stf1Δ
inh1Δ stf1Δ + CCCP
mtDNA/nDNA (normalized to WT without CCCP)
1.5
1.0
0.5
0.0
COX3/ACT1
ATP9/GAL1
I
Ponceau
kDa
70
Cox2
CCCP
- + - +
WT
inh1Δ stf1Δ
Protein level of Cox2 (normalized to WT without CCCP)
1.5
1.0
0.5
0.0
CCCP
- + - +
WT
inh1Δ stf1Δ

Figure 6

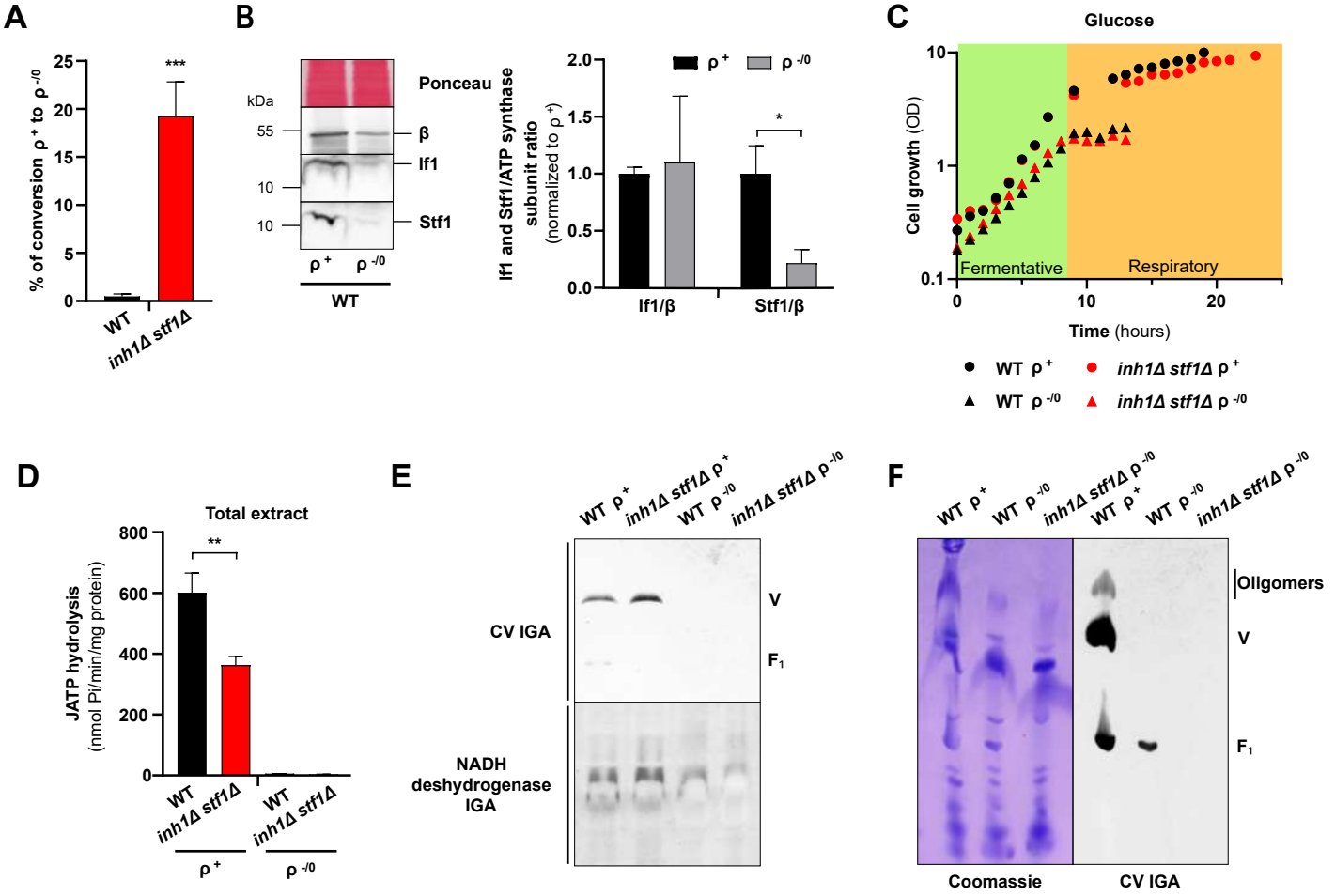
A
% of conversion ρ+ to ρ-/0
25
20
15
10
5
0
***
WT
inh1Δ stf1Δ
B
kDa
55
10
10
Ponceau
β
If1
Stf1
ρ+
ρ-/0
WT
If1 and Stf1/ATP synthase subunit ratio (normalized to ρ+)
2.0
1.5
1.0
0.5
0.0
ρ+
ρ-/0
*
If1/β
Stf1/β
C
Glucose
Cell growth (OD)
10
1
0.1
Fermentative
Respiratory
0
10
20
Time (hours)
WT ρ+
inh1Δ stf1Δ ρ+
WT ρ-/0
inh1Δ stf1Δ ρ-/0
D
Total extract
JATP hydrolysis (nmol Pi/min/mg protein)
800
600
400
200
0
**
WT
inh1Δ stf1Δ
WT
inh1Δ stf1Δ
ρ+
ρ-/0
E
WT ρ+
inh1Δ stf1Δ ρ+
WT ρ-/0
inh1Δ stf1Δ ρ-/0
CV IGA
V
F1
NADH deshydrogenase IGA
F
WT ρ+
WT ρ-/0
inh1Δ stf1Δ ρ-/0
WT ρ+
WT ρ-/0
inh1Δ stf1Δ ρ-/0
Oligomers
V
F1
Coomassie
CV IGA

Supplemental Figure 1

S1A

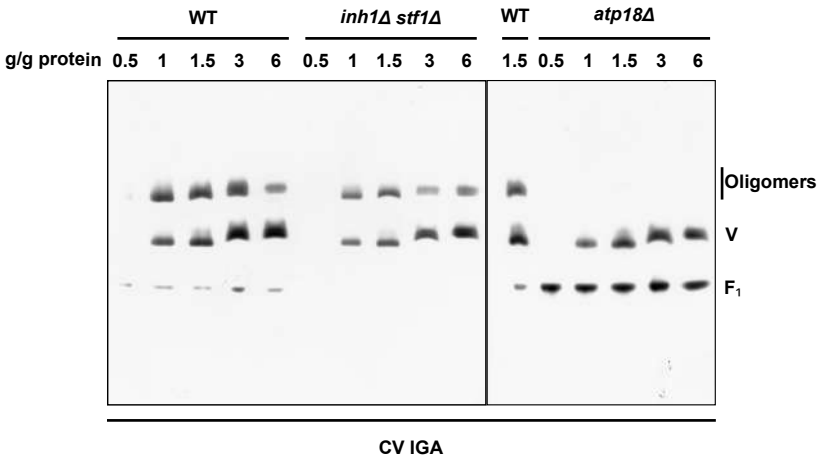

S1B

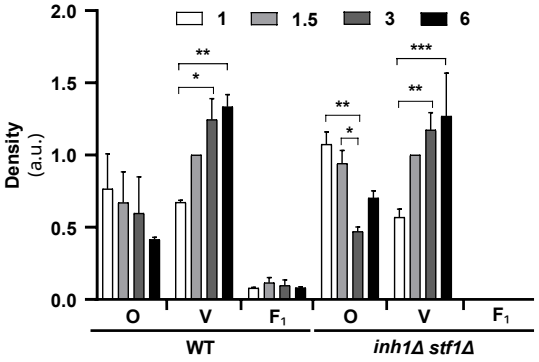

Supplemental Figure 3

S3A

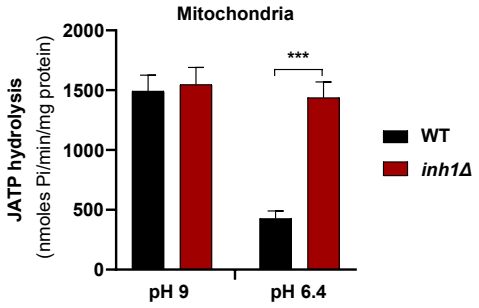

Supplemental Figure 4

S4A

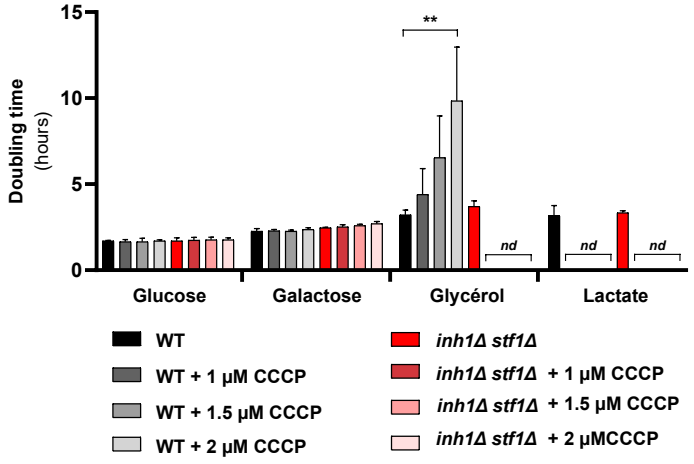
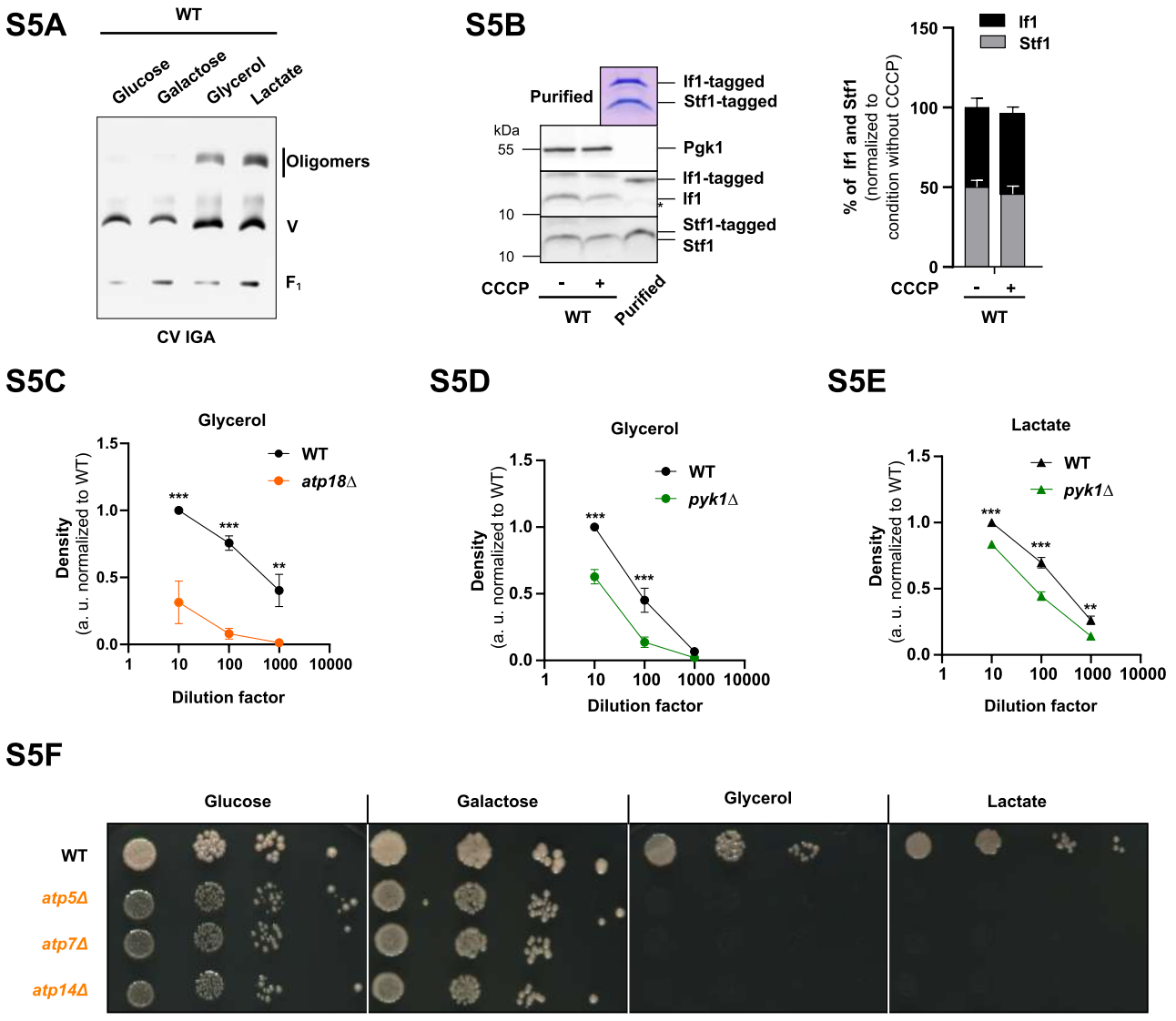
Supplemental Figure 5